Research Square

Preprints are preliminary reports that have not undergone peer review.
They should not be considered conclusive, used to inform clinical practice,
or referenced by the media as validated information.

The Chromatin Accessibility-Associated E2F1–TXNIP Axis Mediates Pulmonary Hypoxic Adaptation in Plateau Cattle by Regulating Bovine Pulmonary Cell Apoptosis

Meiying Zhou
Beijing Jiaotong University
Runcandan A
Beijing Jiaotong University
Riqimuge Ge
Beijing Jiaotong University
Ruina Ma
Beijing Jiaotong University
Gong Chen
Beijing Jiaotong University
Yuze Yang
Beijing Jiaotong University
Junping Li
Beijing Jiaotong University
Bin Li
Tibet Academy of Agricultural and Animal Husbandry Sciences
Yachun Wang
China Agricultural University
Qing Xu
Beijing Jiaotong University
Lingling Hou
llhou@bjtu.edu.cn

Beijing Jiaotong University

Research Article

Keywords: hypoxic adaptation, bovine lung, chromatin accessibility, key genes, oxidative stress, apoptosis

Posted Date: November 25th, 2026

DOI: https://doi.org/10.21203/rs.3.rs-11668017/v1

License: This work is licensed under a Creative Commons Attribution 4.0 International License.
Read Full License

Additional Declarations: No competing interests reported.

The Chromatin Accessibility-Associated E2F1–TXNIP Axis Mediates Pulmonary Hypoxic Adaptation in Plateau Cattle by Regulating Bovine Pulmonary Cell Apoptosis

Meiying Zhou[1], Aruncandan[1], Geriqimuge[1], Ruina Ma[1], Gong Chen[1], Yuze Yang[1], Junping Li[1]， Bin Li[2], Yachun Wang[3], Qing Xu[1*], Lingling Hou[1*]

(1. College of Life Sciences and Bioengineering, Beijing Jiaotong University, Beijing 100044, China; 2. Institute of Animal Husbandry and Veterinary, Xizang Academy of Agricultural and Animal Husbandry Sciences, Lhasa 850000, China; 3. College of Animal Science and Technology, China Agricultural University, Beijing 100193, China)

E-mail:

Meiying Zhou: 24121618@bjtu.edu.cn; Aruncandan: 25121543@bjtu.edu.cn; Geriqimuge: 23121759@bjtu.edu.cn; Ruina Ma: 24121609@bjtu.edu.cn; Gong Chen: cheng265@mail2.sysu.edu.cn; Yuze Yang: 230269614@seu.edu.cn; Junping Li: 26121246@bjtu.edu.cn; Bin Li: xukesuolibin@163.com; Yachun Wang: wangyachun@cau. edu.cn;

*Corresponding author: Qing Xu: qingxu@bjtu.edu.cn; Lingling Hou: llhou@bjtu.edu.cn

Abstract

【Background】The extreme hypoxic environment of the Qinghai-Tibet Plateau frequently induces structural damage of animal lung tissues, cellular oxidative stress, and apoptosis. Local plateau cattle have evolved strong pulmonary hypoxia tolerance, yet the underlying epigenetic mechanisms are not fully understood. **【Results】** this study integrated the assay for transposase-accessible chromatin using high-throughput sequencing (ATAC-seq) with transcriptomic sequencing (RNA-seq) to comprehensively investigate changes in chromatin accessibility and related gene expression during hypoxic adaptation in the lungs of high-altitude cattle. A total of 6,508 differentially accessible chromatin regions were identified and annotated to 560 differentially expressed genes. Motif, Gene ontology and Kyoto Encyclopedia of Genes and Genomes analyses revealed enrichment of hypoxia-related cis-elements and pathways, including apoptosis, autophagy, MAPK, VEGF and PI3K-Akt, with TXNIP identified as a core candidate gene. Based on bovine pulmonary myofibroblasts hypoxia model, we validated that hypoxia treatment significantly inhibited pulmonary cell proliferation, disrupted mitochondrial ultrastructure, reduced mitochondrial membrane potential, and ROS accumulation, while simultaneously activating cellular glycolysis and leading to substantial lactate accumulation. Hypoxia-induced glycolysis can remodel chromatin accessibility in the TXNIP promoter region, allowing the transcription factor E2F1 to directly bind to the open regions and positively activate TXNIP transcription. Increased TXNIP expression can bind and inhibit TRX2,

releasing free ASK1, which further activates the pro-apoptotic p38/Caspase-3 cascade.

【**Conclusions**】This work defines an epigenetic redox axis governing pulmonary hypoxic adaptation in large animals, offering new mechanistic insights and potential targets for hypoxic lung injury.

Keywords: hypoxic adaptation; bovine lung; chromatin accessibility; key genes; oxidative stress; apoptosis

Introduction

The Qinghai-Tibet Plateau, with an average altitude exceeding 4,000 m, is characterized by low atmospheric pressure, hypoxia, and intense ultraviolet radiation. The oxygen partial pressure is only about 60% of that at sea level, and the extremely hypoxic environment severely affects the survival homeostasis of plateau animals(ref. 1). Native plateau animals such as yaks and humped cattle have evolved stable physiological adaptation mechanisms through long-term natural selection and adaptive evolution, making them ideal models for investigating the hypoxic adaptation mechanisms in plateau mammals(ref. 2). As the primary organ for gas exchange and the regulation of oxygen metabolism, the lungs are highly sensitive to hypoxic stress. Structural remodeling, physiological compensation, and metabolic reprogramming of the lungs constitute the fundamental basis for the body's adaptation to the high-altitude hypoxic environment(ref. 3). Compared with the stable adaptive phenotype of high-altitude native cattle, low-altitude animals fail to activate efficient compensatory regulatory mechanisms when exposed to the hypoxic environment of the plateau. Under hypoxic conditions, pulmonary arterial smooth muscle cells are susceptible to pathological changes such as oxidative stress dysregulation, apoptosis, and inflammatory responses, which seriously threaten survival and physiological homeostasis(ref. 4). Therefore, elucidating the molecular mechanisms underlying the hypoxic response in the lungs of high-altitude cattle is of great significance for understanding the adaptive mechanisms of high-altitude mammals, improving the

prevention and control of hypoxic injury at high altitudes. Furthermore, it provides a theoretical basis for the genetic improvement of high-altitude cattle and the development of livestock production in high-altitude regions.

The hypoxic environment of the plateau induces structural, functional, and metabolic remodeling of the bovine lung, resulting in a specific hypoxia-adaptive phenotype. High-altitude cattle adapt to hypoxia by increasing alveolar number, enhancing pulmonary capillary density, and thinning the air-blood barrier to improve gas exchange efficiency, while simultaneously stabilizing pulmonary hemodynamics by thickening pulmonary arteriolar walls and increasing vascular smooth muscle content, thereby adapting to the oxygen supply and circulatory demands of the hypoxic environment(ref. 5, 6). At the metabolic level, hypoxia can trigger pulmonary metabolic reprogramming by inhibiting oxidative phosphorylation and activating anaerobic glycolytic pathways mediated by PDK1 and LDHA(ref. 7). These metabolic adaptations synergistically enhance lipid metabolism and antioxidant pathways, compensating for hypoxia-induced energy metabolic deficits, alleviating oxidative damage, and maintaining pulmonary cellular homeostasis. The hypoxic adaptation in the lungs of high-altitude cattle is a complex process regulated by multiple genes and pathways in a coordinated manner in which a signaling network centered on HIF-1α, together with conserved functional genes such as EPAS1 and EGLN1, plays a key role in hypoxia sensing and signal transduction(ref. 8, 9). Meanwhile, genes from the CDH and COL families are involved in maintaining alveolar-capillary barrier homeostasis and extracellular matrix

remodeling(ref. 10, 11). In addition, multiple pathways such as JAK/STAT, PI3K/Akt, and calcium signaling, collaboratively regulate pulmonary cell proliferation and remodeling, energy metabolism, and immune homeostasis, collectively forming a complex hypoxia regulatory system(ref. 12, 13). Existing studies have mostly focused on gene sequence variations and expression differences, primarily relying on genomic and transcriptomic technologies to characterize the functions of coding genes; however, the epigenetic regulatory mechanisms acting upstream of the hypoxic response remain poorly investigated in a systematic and in-depth manner.

Epigenetic regulation serves as a central bridge linking the environment to gene-specific expression. Chromatin accessibility is an important component of epigenetics and can directly reflects the influence of chromatin structural modifications on gene transcription(ref. 14). Detecting transposase-accessible chromatin by ATAC-seq has become a powerful tool for studying chromatin accessibility, which is widely used to discover different cis-regulatory elements and predict transcription factor binding sites. Wang et al. analyzed eight bovine tissues using ATAC-seq technology and identified 54 key regulatory genes involved in skeletal muscle development, providing a reference for investigating the molecular mechanisms of skeletal muscle development(ref. 15). Building on this, Su et al. identified 17,460 differentially accessible regions and 3,732 differentially expressed genes in sheep skeletal muscle satellite cells using ATAC-seq technology, and screened for candidate genes FZD5 and MAP2K6 that affect the proliferation and differentiation of skeletal muscle satellite cells(ref. 16). Furthermore,

Xu et al. found 47 co-regulated genes, and determined PVALB as a key hub gene when analyzing the longissimus dorsi muscle of selenium-rich black pigs using ATAC-seq technology, thereby providing new insights into the regulatory mechanisms of intramuscular fat deposition(ref. 17). Zhang et al. utilized ATAC-seq technology to analyze endometrial tissue from Meishan and Duroc pigs and found that Meishan pigs exhibited a greater number of open chromatin regions. They identified transcription factors such as Dux, LBX2, and Lhx8, as well as differentially expressed genes including SOX17, ANXA4, and DLX3, thereby revealing the chromatin accessibility landscape and molecular mechanisms underlying the differences in reproductive performance between the two pig breeds(ref. 18). In the study of high-altitude adaptation mechanisms, Lyu et al. used ATAC-seq technology to analyze lung tissue and blood samples from yak and Tibetan yellow cattle on the Qinghai-Tibet Plateau, constructing a chromatin accessibility map and revealing evidence of recent natural selection and genetic introgression from yak in Tibetan yellow cattle(ref. 19). In this study, plateau humped cattle and plain-dwelling Jinnan cattle were selected as research subjects. Humped cattle, a breed developed through long-term selective breeding after the spontaneous crossbreeding of zebu bulls introduced from India and Bhutan with native plateau yellow cattle, possess strong adaptability to the plateau environment. As one of the traditional yellow cattle breeds in the agricultural regions of North China, Jinnan cattle have lived in the Jinnan Basin for a long time and are representative of plain environments. Chromatin accessibility analysis helps identify gene expression

regulatory regions associated with hypoxic adaptation in the lungs of plateau cattle. This contributes to a deeper understanding of gene regulatory networks and is of great significance for revealing differences in chromatin accessibility between plateau and plain cattle.

Thioredoxin-interacting protein (TXNIP) is a multifunctional protein that participates in various biological processes such as oxidative stress, metabolic regulation, immune modulation, and tumor suppression by inducing apoptosis(ref. 20). Furthermore, TXNIP also exerts its regulatory functions through non-apoptotic pathways, such as directly modulating glucose metabolism, inducing ferroptosis, and promoting autophagy(ref. 21, 22, 23). As a tumor suppressor, the pro-apoptotic effects TXNIP have been validated in various cancers such as breast cancer, colorectal cancer, lung cancer, and liver cancer(ref. 20, 24). In addition, Dai et al. found that TXNIP upregulation in mouse podocytes and renal tissue significantly increased ROS production and activated the NLRP3 inflammasome, thereby exacerbating the damage caused by diabetic nephropathy(ref. 25). Similarly, in mouse liver tissue and macrophages, increased TXNIP expression can activate the NLRP3 inflammasome to mediates inflammatory responses, thereby aggravating oxidative stress-induced hepatotoxicity(ref. 26). In LPS-induced acute lung injury, Wang et al. demonstrated that ROS triggered the dissociation of TXNIP from Trx-1. After that TXNIP binded to and activated the NLRP3 inflammasome, thereby promoting the secretion of IL-1β and IL-18 as well as inducing pyroptosis, ultimately worsening inflammatory injury(ref. 26,

27). Zhang et al. found that TXNIP expression was significantly upregulated under hypoxic conditions through experiments using human pulmonary artery endothelial cells and lung tissues from mice with hypoxia-induced pulmonary arterial hypertension. TXNIP further exacerbates oxidative stress, inflammatory responses, and mitochondrial autophagy by activating the NLRP3 inflammasome , ultimately leading to pulmonary vascular endothelial dysfunction and vascular remodeling(ref. 28). In contrast, downregulation of TXNIP expression attenuates apoptosis and inflammation. Zhao et al. demonstrated that knocking down TXNIP in rat spinal cord and PC12 cells can inhibit bupivacaine-induced oxidative stress and apoptosis, thereby protecting neuronal function in the spinal cord(ref. 29). Similarly, Wang et al. also found reducing TXNIP expression in the islets of diabetic mice effectively decreased pancreatic β-cell apoptosis and inflammatory responses, which were also observed in the islets of diabetic mice(ref. 30). Collectively, these findings indicate that TXNIP is a critical regulatory factor linking hypoxia, oxidative stress, and apoptosis. However, the epigenetic regulatory mechanisms of TXNIP during the hypoxic response in the lungs of high-altitude cattle, as well as its role in modulating apoptosis, remain poorly understood.

This study analyzed differences in chromatin accessibility of lung tissues between plateau cattle and plain cattle using ATAC-seq technology, screened for key genes related to hypoxia adaptation and further explored the underlying molecular mechanisms by which the key gene TXNIP mediates hypoxic adaptation of lung cells.

The study provides experimental evidence for a deeper understanding of the epigenetic regulatory mechanisms of hypoxia adaptation in plateau mammals, and also offers theoretical basis for the prevention and control of hypoxia stress in plateau livestock, genetic improvement of germplasm, and research on high-altitude lung injury in humans.

Result

Result 1. ATAC-seq Data Quality Assessment and Chromatin Accessibility Profiling of Lung Tissues from Hump Cattle and Jinnan Cattle

ATAC-seq libraries prepared from lung tissue (LU) of high-altitude Hump Cattle (TF, n = 5) and lowland Jinnan Cattle (JN, n = 5) were sequenced on the Illumina NovaSeq 6000 platform to generate 150-bp paired-end reads. A total of 163.28 Gb of raw sequencing data was obtained from the 10 samples. Following removal of adapter sequences and low-quality reads, an average of 54,424,863.2 raw reads was retained per sample, with a mean clean-read ratio of 70.32%. The mean Q20 and Q30 values were 96.88% and 91.67%, respectively (Table 1-1). Overall, these quality-control results indicated that the ATAC-seq datasets were of sufficient quality for subsequent downstream analyses.

Table 1-1. Quality Control Metrics of the ATAC-seq Data

Sample	Raw _data	Raw_bases(G)	Clea _data	Clean_bases(G)	Clean_ratio	Q20	Q30
JN_1_LU	48060262	14.42	47617161	11.02	76.42%	96.75%	90.70%
JN_2_LU	55046672	16.51	54326551	11.20	67.84%	97.10%	91.95%

JN_3_LU	43117377	12.94	42326425	8.45	65.30%	97.65%	93.49%
JN_4_LU	72294673	21.69	71042549	14.68	67.68%	96.90%	91.76%
JN_5_LU	45984472	13.80	45462720	8.53	61.81%	97.56%	93.26%
TF_1_LU	71709790	21.51	70146994	15.76	73.27%	96.72%	91.36%
TF_2_LU	49766805	14.93	48045764	10.59	70.93%	96.94%	92.25%
TF_3_LU	54702093	16.41	53443726	12.04	73.37%	96.48%	90.92%
TF_4_LU	71358391	21.41	70395964	13.87	64.78%	97.21%	92.36%
TF_5_LU	32208097	9.66	31545688	7.9	81.78%	95.51%	88.68%

Table legend: Summary of sequencing raw data, clean data ratio and quality values (Q20, Q30) for ATAC-seq libraries. LU indicates lung tissue sample; Raw_data, total number of raw sequencing reads; Raw_bases(G), total raw sequencing bases in gigabases; Clean_data, read count after removing adapters and low-quality reads; Clean_bases(G), clean sequencing bases in gigabases; Clean_ratio, proportion of clean reads; Q20 and Q30 represent the percentage of bases with Phred quality score ≥20 and ≥30, respectively. TF: plateau humped cattle; JN: plain Jinnan cattle. n = 5 biological replicates for each group.

The clean reads generated from ATAC-seq analysis of lung tissues from high-altitude and lowland cattle were aligned to the bovine reference genome (Bos_taurus.ARS-UCD1.2). The mean unique mapping rate across all samples was 81.40% (Unique_ mapped), indicating robust mapping efficiency and good alignment quality. The resulting datasets were therefore suitable for subsequent downstream analyses (Table 1-2).

Table 1-2. Alignment Results of ATAC-seq Data

Sample	Clean_reads	Mapped_MT_PT	Mapped_non_MT_PT	Unique _mapped
JN_1_LU	47617161	2306783(4.96%)	44209751 (92.84%)	33950213(76.79%)
JN_2_LU	54326551	1547644(2.85%)	51503527 (90.80%)	41019704 (79.64%)
JN_3_LU	42326425	1622857(3.83%)	39856311 (94.16%)	30920934 (77.58%)
JN_4_LU	71042549	6032158(8.49%)	63896470 (89.94%)	53536605 (83.79%)
JN_5_LU	45462720	2274912(5.06%)	41661909 (91.64%)	33045667 (79.32%)
TF_1_LU	70146994	6490025(9.25%)	62327983 (88.85%)	52851733 (84.80%)
TF_2_LU	48045764	1518651(3.16%)	45212044 (94.10%)	36483250 (80.69%)
TF_3_LU	53443726	7176180(13.43)	44889161 (83.99%)	38172590 (85.04%)
TF_4_LU	70395964	4851848(6.89%)	63353677 (90.00%)	50905263 (80.35%)
TF_5_LU	31545688	2172258(6.89%)	28641187 (90.79%)	24633268 (86.01%)

Table legend: Alignment outputs of clean ATAC-seq reads. Clean_reads: filtered high-quality sequencing reads; Mapped_MT_PT: reads mapped to mitochondrial or plastid sequences; Mapped_non_MT_PT: reads mapped to nuclear genome excluding mitochondria; Unique_mapped: uniquely mapped reads used for subsequent peak calling. Values in parentheses represent corresponding percentage. TF: plateau humped cattle; JN: plain Jinnan cattle; LU: lung tissue. n = 5 per group.

Further analysis of inserted fragment distributions revealed a characteristic periodicity of approximately 200 bp across all samples. A prominent first peak was significantly enriched in fragments shorter than 200 bp, corresponding to the nucleosome-free region (NFR) (Figure 1A) (Supplementary Figure 2), whereas the periodic peaks reflected the presence of nucleosomes in chromatin structure and their regular arrangement. This fragment-size distribution was consistent with the

characteristic pattern of ATAC-seq libraries.

Building on these findings, we further characterized the distribution of chromatin-accessible regions relative to transcription start sites (TSSs) in plateau and plain cattle. The results showed that chromatin-accessible regions were significantly enriched within 3 kb upstream and downstream of the TSS in both group, with enrichment signals progressively increasing as the distance to the TSS decreased (Figures 1B, C). Notably, chromatin-accessible regions were predominantly concentrated within 0–1 kb of the TSS, accounting for an average of 38.19% of the total accessible regions (Figures 1D, E) (Supplementary Figure 3). Genomic annotation of chromatin-accessible regions revealed that these regions of the two groups were predominantly located in promoter, intergenic, and intronic regions. The mean proportion of accessible regions annotated to promoters was 40.29% in high-altitude cattle and 47.34% in lowland cattle, indicating a notable difference between the two groups. In contrast, the proportions of accessible regions annotated to intergenic and intronic regions were very similar between the two groups of samples, with highland cattle being slightly higher than plain cattle. Specifically, the average proportion for highland cattle was 31.20%, and 29.06% for plain cattle; whereas the corresponding proportions for intronic regions were 21.99% and 19.76%, respectively (Figure 1F) (Supplementary Figure 4). Collectively, these findings indicate distinct there are differences in chromatin accessibility profiles between plateau cattle and plain cattle. Differential chromatin accessibility was predominantly observed in promoter, intergenic, and intronic regions, with promoter

regions representing the largest proportion which suggests that promoter-proximal chromatin accessibility, particularly within 1 kb of the TSS, may play an important role in transcriptional regulation. Further analysis of peak distributions across chromosomes showed that accessible chromatin peaks were broadly distributed across all chromosomes, with substantially greater peak coverage in plateau cattle than in plain cattle (Figure 1G) (Supplementary Figure 5). These findings suggest that high-altitude cattle possess a more open chromatin landscape, which may contribute to their adaptation to hypoxic environments.

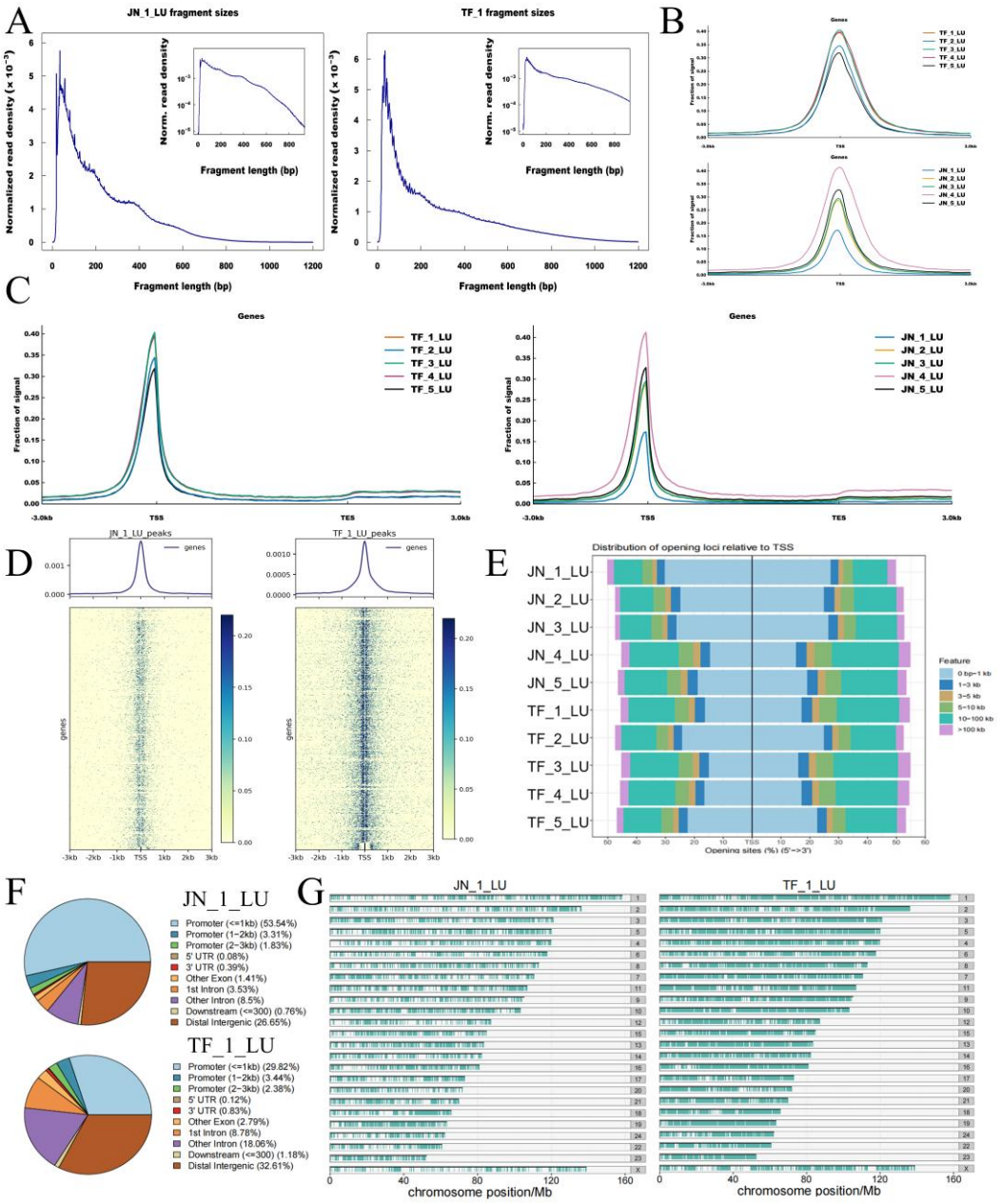


Figure 1. ATAC-seq profiling and chromatin accessibility characteristics of lung tissues from Hump Cattle and Jinnan Cattle.

(A) Distribution of inserted fragment sizes in TF_LU and JN_LU samples. (B) Distribution of chromatin accessibility signals around transcription start sites (TSSs). (C) TSS enrichment profiles and enrichment of nucleosome-free fragments at TSSs. (D) Genomic distribution of ATAC-seq peaks in TF_LU and JN_LU samples. Genomic

regions were classified into promoters, 5′ untranslated regions (5′UTRs), coding exons, introns, 3′ untranslated regions (3′UTRs), and distal intergenic regions, as indicated by the labels and colors above the stacked bar plots. (E) Peak annotation pie chart of genomic annotation of ATAC-seq peaks, more than half of the peaks are located in intergenic, intronic, and promoter regions. (F) Distribution of ATAC-seq peaks on chromosomes in TF_LU and JN_LU samples.

Result 2. Functional Enrichment of Differentially Accessible Regions and Identification of Key Candidate Genes

DESeq2 was used to identify differentially accessible regions (DARs) in lung tissues from high-altitude and plain cattle. Using the criteria of $|\log_2 FC| > 1$ and $P < 0.05$, 6,508 DARs were identified, corresponding to 560 annotated genes. Among these DARs, 5,787 showed increased chromatin accessibility and were associated with 514 annotated genes, whereas 721 exhibited decreased chromatin accessibility and were associated with 46 annotated genes. In contrast, 107,802 chromatin-accessible regions showed no significant differences between the two groups (Figure 2A).

Further analysis showed that DARs in the promoter region ≤1Kb from TSS were annotated to 358 related genes. Gene Ontology (GO) enrichment analysis identified a total of 46 significantly enriched GO terms, including 9 Molecular Function (MF), 24 Biological Process (BP), and 13 Cellular Component (CC) terms, closely associated with adaptation to high-altitude hypoxia adaptation (Figure 2B). Among the BP terms, significantly enriched terms included small GTPase-mediated signal transduction,

negative regulation of endothelial cell proliferation, positive regulation of angiogenesis, positive regulation of DNA-templated transcription, and regulation of transcription by RNA polymerase II. For the CC category, significantly enriched terms included Golgi membrane, Golgi apparatus, early endosome, recycling endosome, cytoskeleton, cis-Golgi network, cytoplasmic vesicle, and histone deacetylase complex. The enrichment of these cellular components suggests that DAR-associated genes involved in macromolecular metabolism, and transcriptional regulation may play important functions during hypoxic adaptation of high-altitude cattle lung. For the MF category, significantly enriched terms included transcription corepressor activity, GTPase-activating protein binding, cysteine-type endopeptidase activity, GTPase activator activity, protein binding, and protein serine/threonine kinase activity. Among these, GTPase activator activity, GTPase-activating protein binding, and protein serine/threonine kinase activity are closely associated with hypoxia-responsive signaling, angiogenesis, and downstream signal transduction. In summary, the GO enrichment analysis results reveal that DARs-related genes may mediate the adaptive regulation of high-altitude cattle lung tissues to the hypoxic environment by participating in multiple processes such as hypoxic stress response angiogenesis, energy metabolism, and signal transduction.

KEGG pathway enrichment analysis was performed on the 358 DARs genes, identifying a total of 240 enriched pathways, among which 66 were significantly enriched and involved 93 genes. Among these, 15 pathways have been previously

reported to be closely associated with high-altitude hypoxia adaptation (Figure 2C). These pathways encompassed multiple key biological processes, including core signal transduction, energy metabolism and apoptosis, and regulation of pulmonary vascular function. It reflects the complex adaptive mechanisms of lung tissue in response to a high-altitude hypoxic environment.

Notably, the top 10 most significantly enriched KEGG pathways were predominantly associated with hypoxia adaptation (Figure 2D). These pathways were mainly involved in cytoskeleton rearrangement, cell junction assembly and multiple signaling transduction. Among them, adherens junction and regulation of actin cytoskeleton were prominently enriched, implying their potential roles in maintaining pulmonary tissue structure and vascular remodeling during high-altitude hypoxic adaptation. Furthermore, the significant enrichment of inflammatory signaling pathways, including the NOD-like receptor and Toll-like receptor pathways, indicates that immune activation and the maintenance of immune homeostasis are indispensable aspects of hypoxic adaptation.

To further characterize the functions relationships and interactions among DAR-related genes, protein–protein interaction (PPI) network analysis was performed on the 358 DAR-associated genes using the STRING database. The top 100 genes ranked by degree value visualized using Cytoscape (Figure 2E). Core nodes located at the center of the network include MAPK1, CDH1, BIRC5, FGF9, MRPL13, and others, which serve as central hubs of the interaction network. As a signaling integration hub for

hypoxic stress, MAPK1 can both activate Mtorc1 and synergize with the PI3K-Akt pathway to promote protein synthesis and cell survival, while also inhibiting the FoxO pathway to suppress antioxidant enzyme expression, thereby driving cells toward apoptosis. In addition, MAPK1 is involved in VEGF-mediated signaling and may cooperate with cell adhesion and Toll-like receptor signaling to regulate angiogenesis and immune responses. CDH1 inhibits Caspase-3/7 activation by binding to BIRC5, thereby resisting hypoxia-induced alveolar epithelial apoptosis and maintaining the integrity of cell adhesion junctions. FGF9 regulates of the Rap1 and Wnt pathways and participates in cell adhesion, migration, tissue homeostasis, and regeneration. In addition, multiple key genes are involved in the lung's hypoxic response. MAPK1 mediates pulmonary vascular endothelial proliferation and remodeling; whereas downregulation of CDH1 expression disrupts the alveolar epithelial barrier, contributing to high-altitude pulmonary edema and pulmonary fibrosis. CASP8 is involved in extrinsic apoptosis and inflammasome activation, participating in hypoxic lung injury. TXNIP regulates the thioredoxin system, mediating ROS production and ferroptosis to maintain redox homeostasis. CXCR4 participates in pulmonary vascular endothelial migration and angiogenesis, while CCND2 regulates cell-cycle progression and promotes the survival and proliferation of pulmonary cells under hypoxic conditions. These hub genes are involved in multiple biological processes, including pulmonary vascular remodeling, epithelial barrier maintenance, apoptosis, oxidative stress, cell-cycle regulation, and inflammatory responses, collectively forming the key

molecular basis for pulmonary adaptation to high-altitude hypoxia.

Motif enrichment analysis of the DARs identified 286 significantly motifs ($P < 0.05$), indicating that DARs possess complex sequence regulatory features. Among the top 50 candidate transcription factors, HIF-1α emerges as a prominent regulator of the hypoxic response and plays a regulatory role in pulmonary vascular remodeling, alveolar epithelial cell injury, and apoptosis. It is also a key regulatory molecule in high-altitude hypoxia lung injury and pulmonary hypertension. The transcription factors c-Myc, FOXO1, and FOXO3 can bind to E-box cis-regulatory elements to collectively regulate proliferation and apoptosis pulmonary cell. Under hypoxic conditions, FOXO family members have been reported to promote apoptosis in pulmonary epithelial cells by upregulating the expression of BIM1 and BIM3, whereas c-Myc alleviates excessive apoptosis through reverse regulation, thereby maintaining cell survival. FOX family transcription factors, including FOXA1, FOXA2, FOXA3, and FOXM1, are involved in lung development, epithelial differentiation, and tissue repair following injury. Among these factors, FOXM1 can promote the regeneration of pulmonary endothelial cells under hypoxic conditions. Several members of the bZIP family, including ABF1, ABF2, AREB3, ABI5, and bZIP28, can bind to CRE elements to mediate hypoxia-induced oxidative stress and apoptotic signaling pathways in lung cells. USF1, USF2, and TFE3, can target E-box sequences and are involved in metabolic reprogramming and apoptotic regulation of lung cells under hypoxia. In addition, p63 and SIX1 are involved in pulmonary stem/progenitor cell differentiation and tissue repair following

lung injury, whereas CLOCK may contribute to the regulation of circadian rhythm to hypoxic stress. The 10 most significantly enriched motifs and their corresponding candidate transcription factors are summarized in Table 1-3. Notably, six of the top 10 motifs contained the core sequence “CACGTG”, which is characteristic of the Coordinated Lysosomal Expression and Regulation (CLEAR) element, suggesting that CLEAR-like regulatory sequences are widely present in differentially accessible chromatin regions. Previous studies have shown the CLEAR element is an important regulatory sequence for lysosome-associated genes. Transcription factors capable of recognizing CLEAR-related motifs, such as TFE3 from the TFE family and Bhlh18 from the bHLH family, can regulate lysosome biogenesis, thereby affecting the mitochondrial-mediated apoptotic pathway. In addition, it has been reported that FOXA2 and BIM play important roles in regulating cell apoptosis under hypoxic conditions.

Table 1-3. Motif Enrichment Analysis of DARs and Prediction of Candidate Transcription Factors

Motif	Match TF	P-value	% of Target
	E-box	1e-898	13.18%
	TFE3	1e-884	13.83%
	bHLH18	1e-792	8.59%
	BIM3	1e-713	14.66%
	BIM1	1e-700	14.11%

	Fox:Ebox	1e-531	42.66%
	FOXA1	1e-505	43.52%
	Foxa3	1e-493	20.90%
	PIF7	1e-486	15.96%
	Foxa2	1e-465	36.72%

Table legend: Transcription factors predicted to bind to the 472-bp differential accessible region within the TXNIP gene promoter. Match TF: candidate transcription factor; P-value: motif enrichment significance; % of Target: proportion of target sequences carrying the corresponding motif.

To further characterize the functional relevance and potential interactions of DAR-associated genes, we integrated the PPI network and KEGG enrichment results to identify candidate core genes. First, the top 100 genes with the highest degree values in the PPI network were selected and intersected with the 93 genes involved in the 66 significantly enriched KEGG pathways ($P < 0.05$), yielding 39 core DAR-associated genes. These 39 genes were subsequently prioritized according to three complementary criteria: transcriptomic fold change, the number of significantly enriched KEGG pathways in which each gene was involved, and ATAC-seq read counts expressed as reads per million (RPM). The top 25 genes ranked according to each criterion were intersected, resulting in the identification of 13 key genes potentially associated with hypoxic adaptation in bovine lung tissue (Figure 2F).

To further investigate the enrichment of DAR-associated key genes in chromatin

accessibility signals. Integrative Genomics Viewer (IGV) was used to visualize the ATAC-seq profiles of the housekeeping gene GAPDH and the DAR-associated key genes TXNIP, WASF2, B2M, EIF3H, and NRP1. The results showed that enrichment peaks were observed upstream of the TSS of all the above genes. The housekeeping gene GAPDH exhibited no significant differences in sequencing peak height and coverage breadth across all samples in both groups, supporting the overall comparability of sequencing depth and chromatin accessibility profiles between the Hump cattle and Jinnan cattle groups. The genomic ATAC-seq profiles of NRP1, EIF3H, B2M, and WASF2 exhibited broadly similar peak patterns and enrichment intensities between the TF and JN groups, with relatively weak overall signal coverage and no obvious differences between groups.In contrast, TXNIP displayed a pronounced difference in ATAC-seq signal intensity between the two groups. In the JN group, the TXNIP locus of the JN group exhibited relatively low peak intensity and weak overall signal coverage. In the TF group, markedly stronger ATAC-seq peaks were observed in the promoter and coding regions of TXNIP, with substantially greater fragment enrichment than that observed in the JN group, which provides visual evidence that the TXNIP locus exhibits higher chromatin accessibility in the TF group than in the JN group (Figure 2G).

To further investigate the potential roles and mechanisms of DAR-associated key genes in the hypoxic adaptation of bovine lung tissue, the expression of seven DAR-associated key genes identified through ATAC-seq, including HSPA6, TXNIP,

NEDD4L, WASF2, EIF3H, NRP1, and B2M, was detected in bovine pulmonary cells under hypoxic conditions using RT-qPCR. Compared with the normoxic control group maintained at 21% O_2, bovine pulmonary myofibroblasts cultured under 1% O_2 for 72 h exhibited distinct changes in the expression of these candidate genes (Figure 2H). The expression levels of TXNIP and NRP1 were significantly upregulated, whereas those of NEDD4L, WASF2, B2M, and EIF3H were significantly downregulated. No significant change was observed in HSPA6 expression. Notably, the marked upregulation of TXNIP under hypoxic conditions was highly consistent with the chromatin accessibility pattern observed in the ATAC-seq data from high-altitude bovine lung tissue, as well as with the expression trend identified in our previous transcriptomic sequencing data. By integrating ATAC-seq data, gene function annotations, and cellular experimental results, it is inferred that TXNIP plays an important role in the hypoxic adaptation process of high-altitude cattle lungs.

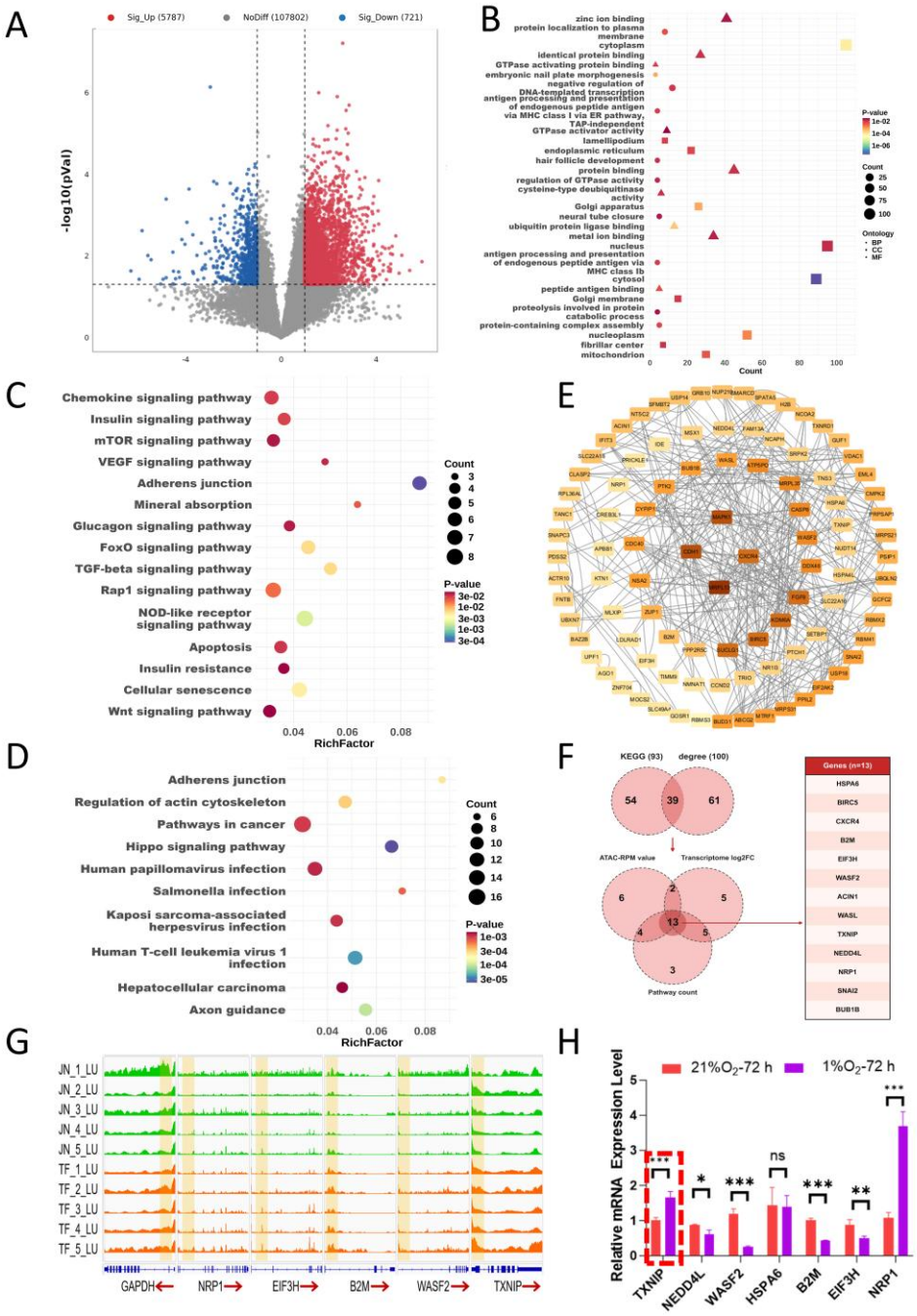


Figure 2. Enrichment analysis of differentially accessible regions and associated genes and identification of key candidate genes.

(A) Volcano plot showing differentially expressed genes (DEGs) between the TF_LU and JN_LU groups. (B) GO enrichment terms associated with hypoxia adaptation among the DEGs. (C) Twenty-two significantly enriched KEGG pathways associated with hypoxia adaptation among the DEGs. (D) Top 20 significantly enriched KEGG

pathways associated with hypoxia adaptation among the DEGs. (E) Protein–protein interaction (PPI) network of DAR-associated genes. (F) Venn diagram illustrating the identification of core candidate genes by integrating ATAC-seq, transcriptomic, and pathway enrichment data. (G) IGV visualization of chromatin accessibility signals at the housekeeping gene GAPDH and representative core genes across all samples. (H) The expression levels of core candidate genes under normoxic conditions and hypoxic exposure after 72 h (*P < 0.05, **P < 0.01; ns, not significant).

Result 3. Prediction and Functional Validation of Transcription Factors Regulating TXNIP Expression

To investigate the transcriptional regulatory mechanisms underlying TXNIP during the hypoxic adaptation of high-altitude bovine lung tissue, we further screened for candidate transcription factors potentially involved in the regulation of TXNIP based on motif enrichment analysis. First, motif enrichment analysis was performed using the JASPAR database on the DARs within the TXNIP promoter region of 472 bp identified from the ATAC-seq data and 209 candidate transcription factors were predicted. We subsequently focused on significantly enriched motifs within these DARs and identified eight transcription factors potentially associated with TXNIP transcriptional regulation: TFE3, FOXO3, c-Myc, FOXO1, KLF5, KLF6, ETS1, and E2F1 (Table 3-1). TFE3 has previously been reported to downregulate TXNIP expression in a diabetic mouse model by binding to the TXNIP promoter region(ref. 31). FOXO3 can promote TXNIP upregulation in mouse microglial cells, thereby exacerbating ROS accumulation and

aggravating spinal cord injury(ref. 32). In triple-negative breast cancer cells with acquired drug resistance, stimulation-induced nuclear translocation of c-Myc activates TXNIP expression, leading to increased intracellular ROS levels and metabolic reprogramming(ref. 33). FOXO1 can positively regulate TXNIP expression and promote ferroptosis in mouse muscle satellite cells(ref. 34). Previous studies have confirmed that KLF5 can upregulate TXNIP expression in human ovarian granulosa cells, thereby contributing to apoptosis and inflammatory injury(ref. 35). It has been shown that KLF6 can enhance TXNIP promoter activity in a mouse model of myocardial ischemia–reperfusion injury, thereby worsening tissue injury(ref. 36). In human colon cancer cells, taurine enhances the binding of ETS1 to the TXNIP promoter region and consequently promotes TXNIP expression(ref. 37). Furthermore, E2F1 has been reported to bind to the TXNIP promoter and regulate its expression in several human cell lines such as human endothelial progenitor cells(ref. 38, 39, 40). To further narrow down the candidate transcription factors potentially involved in TXNIP regulation in bovine pulmonary myofibroblasts, the eight transcription factors identified from the ATAC-seq-based motif analysis were intersected with the top 150 transcription factors ranked by JASPAR prediction score among the 209 predicted candidates and identified two overlapping transcription factors, KLF5 and E2F1 (Figure 3A). Functional annotation and literature analysis of these two candidates revealed that E2F1 has been reported to bind the TXNIP promoter in multiple human cell types and positively regulate TXNIP expression, thereby contributing to the regulation of

apoptosis (ref. 38, 39, 40) . In contrast, relatively limited evidence is currently available regarding the direct regulation of TXNIP by KLF5. In summary, it is speculated that E2F1 may also regulate TXNIP in bovine pulmonary myofibroblasts.

Table 3-1. Transcription Factors Potentially Involved in the Regulation of TXNIP

Motif	Match TF	P-value	%of Target
	TFE3	1e-884	13.83%
	Foxo3	1e-346	32.28%
	c-Myc	1e-206	20.55%
	Foxo1	1e-168	50.85%
	KLF5	1e-67	23.92%
	KLF6	1e-30	19.46%
	ETS1	1e-27	7.74%
	E2F1	1e-5	2.88%

In view of these findings, we first examined the expression of E2F1 and TXNIP in bovine pulmonary myofibroblasts under hypoxic conditions by Western blot. Compared with the normoxic control group, both E2F1 and TXNIP protein levels were significantly increased following hypoxic exposure, exhibiting a consistent expression pattern (Figures 3B, C). To further investigate the regulatory relationship between E2F1 and TXNIP, E2F1 expression was suppressed using E2F1-specific siRNA or the E2F1 inhibitor HLM006474. Inhibition of E2F1, either by siRNA-mediated knockdown or inhibitor treatment, resulted in a significant downregulation of TXNIP expression (Figures 3D, G), which suggested that E2F1 might positively regulate TXNIP expression. We subsequently performed a dual-luciferase reporter assay to determine

whether E2F1 directly regulates TXNIP transcription. The 11-bp putative E2F1-binding motif within the TXNIP promoter was completely mutated from “TAAGCGGCAGG” to “TCTATTATCCT”, and the resulting construct was designated the mutant (MT) reporter plasmid. The wild-type (WT) and MT reporter plasmids were transfected into bovine pulmonary myofibroblasts. The WT TXNIP promoter significantly increased luciferase activity, whereas mutation of the E2F1-binding site markedly reduced promoter-driven luciferase activity (Figures 3H, I). These findings provide further evidence that E2F1 positively regulates TXNIP transcription through its binding site within the TXNIP promoter.

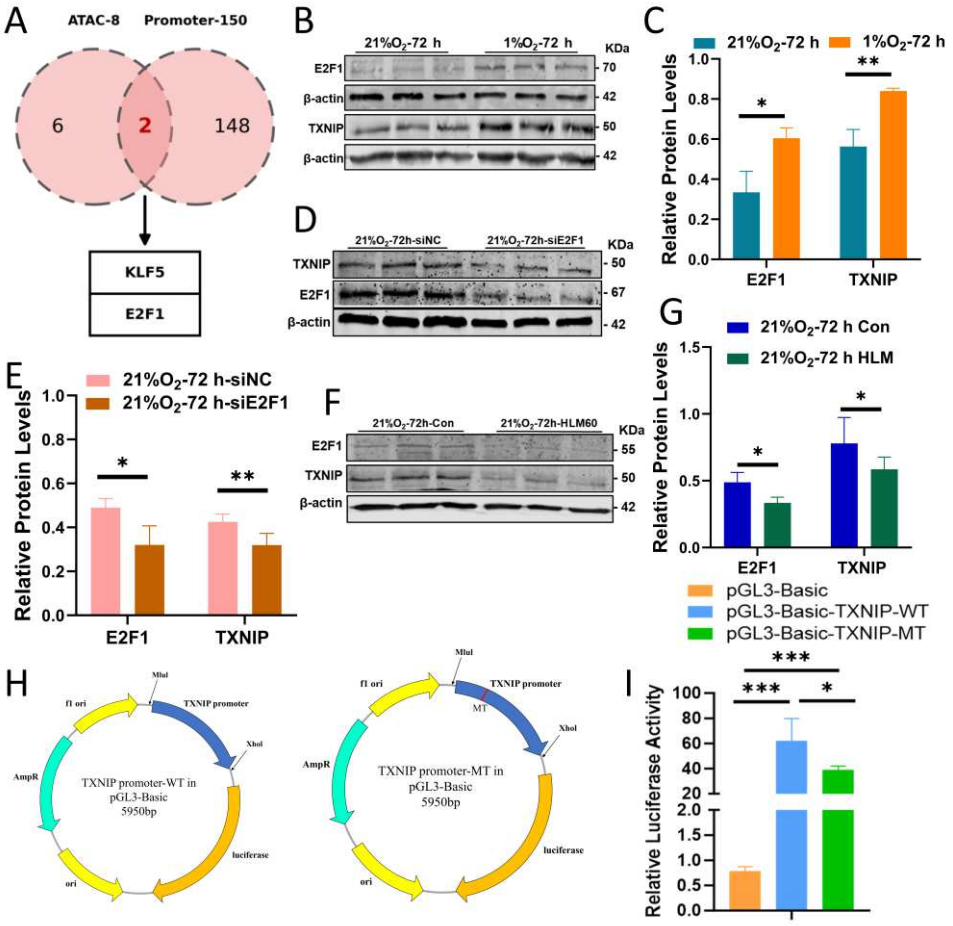


Figure 3. Prediction and functional validation of transcription factors regulating

TXNIP. (A) Venn diagram showing the intersection between transcription factors associated with TXNIP regulation identified by ATAC-seq motif analysis and the top 150 transcription factors predicted by the JASPAR database. (B) Representative Western blot results showing the hypoxia-induced upregulation of E2F1 and TXNIP expression following exposure to 1% O_2 for 72 h (*P < 0.05, **P < 0.01). (C) Quantification of E2F1 and TXNIP protein expression following exposure to 1% O_2 for 72 h. (D) Representative Western blot bands showing E2F1 and TXNIP protein expression following siRNA-mediated knockdown of E2F1. (E) Quantification of E2F1 and TXNIP protein expression following siRNA-mediated knockdown of E2F1. (F) Representative Western blot bands showing E2F1 and TXNIP protein expression following treatment with the E2F1 inhibitor HLM006474. (G) Quantification of E2F1 and TXNIP protein expression following treatment with HLM006474. (H) Schematic representation of the predicted E2F1-binding site within the TXNIP promoter. (I) Dual-luciferase reporter assay confirming the positive regulatory effect of E2F1 on the TXNIP promoter.

Result 4: Effects of Hypoxia on Bovine Pulmonary Myofibroblast Function

To investigate the effects of hypoxia on bovine pulmonary myofibroblasts, 1% O_2 was selected as the hypoxic culture condition based on the physiological oxygen partial pressure of cells, oxygen availability at high altitudes, and hypoxic conditions commonly used in previously reported in vitro hypoxia models.

The effects of hypoxia on the proliferative activity of bovine pulmonary

myofibroblasts were evaluated using the MTT assay following exposure to 1% O_2 for 72 h. The results showed that OD_{490} value was significantly lower in the hypoxic group than in the normoxic control group after 72 h of exposure to 1% O_2 (Figure 4A), indicating that hypoxic exposure significantly suppresses the proliferative activity of bovine pulmonary myofibroblasts.

The effect of hypoxia on the ultrastructure of bovine pulmonary myofibroblasts was observed using transmission electron microscopy (TEM) (Figure 4B). Under normoxic conditions, the nuclear envelope of bovine pulmonary myofibroblasts remained intact, with a uniform perinuclear space and no apparent structural abnormalities. The chromatin was loosely distributed, and the nucleoli exhibited well-preserved morphology, consistent with a normal physiological state. Mitochondria displayed regular morphology with intact double-membrane structures and well-defined cristae. They were predominantly short rod-shaped or oval and evenly distributed throughout the cytoplasm. The rough endoplasmic reticulum exhibited an intact and continuous membrane structure, predominantly arranged in parallel sheets, with ribosomal particles uniformly distributed along its cytoplasmic surface. After exposure to 1% O_2 for 72 h, the cytoplasmic density was markedly reduced, accompanied by pronounced ultrastructural alterations. The nuclear envelope became highly contracted and exhibited conspicuous wrinkling and discontinuities. The endoplasmic reticulum was visibly swollen. In addition, mitochondria showed prominent structural abnormalities, including marked swelling, increased mitochondrial volume, and disorganization of the

cristae. A substantial number of autophagosomes were also observed in the cytoplasm. These findings indicate that prolonged hypoxic exposure induces pronounced alterations in the ultrastructure of bovine pulmonary myofibroblasts, particularly affecting the nuclear envelope, endoplasmic reticulum, and mitochondria.

To further investigate the effects of hypoxia on mitochondrial function in bovine pulmonary myofibroblasts, mitochondrial membrane potential ($\Delta\Psi m$) under hypoxic conditions (1% O_2) was assessed using a fluorescent probe. Compared with the normoxic control group, cells exposed to 1% O_2 for 72 h exhibited an increase in green fluorescence accompanied by a reduction in red fluorescence, indicating a significant decrease in mitochondrial membrane potential following hypoxic exposure (Figure 4C). A reduction in mitochondrial membrane potential is an early indicator of mitochondrial dysfunction and apoptosis, which was consistent with the mitochondrial ultrastructural alterations observed by TEM. To determine whether hypoxia-induced mitochondrial dysfunction was accompanied by increased oxidative stress, intracellular reactive ROS levels were assessed using the DCFH-DA fluorescent probe. Compared with the normoxic control group, ROS production was markedly increased in bovine pulmonary myofibroblasts following exposure to 1% O_2 for 72 h (Figure 4D), suggesting that hypoxic exposure induces obvious oxidative stress and is associated with mitochondrial dysfunction. ROS exert a typical 'double-edged sword' role in cells. Under normal conditions, low concentrations of ROS generated by the mitochondrial respiratory chain can act as second messengers and participate in metabolic signaling and the

maintenance of cellular homeostasis. In contrast, excessive ROS accumulation under hypoxic or other stress conditions can disrupt mitochondrial membrane integrity, impair cellular energy metabolism, and promote apoptotic signaling (ref. 41).Based on these findings, we further investigated the effect of hypoxia on cell apoptosis and autophagy by detecting the expression of autophagy markers p62 and LC3B, as well as apoptosis markers BAX and BCL2 in bovine pulmonary myofibroblasts under hypoxic conditions using western blot. Compared with the normoxic control group, exposure to 1% O_2 for 72 h significantly decreased p62 protein expression, whereas LC3B expression showed no significant change. In addition, BAX expression was significantly increased ($P < 0.05$), whereas BCL2 expression was significantly decreased ($P < 0.05$), resulting in a significant elevation of the BAX/BCL2 ratio (Figures 4.E, F). Comprehensive analysis indicates that hypoxic conditions lead to increased levels of autophagy and apoptosis within cells.

Under hypoxic conditions, cellular energy metabolism undergoes metabolic reprogramming, with a shift from oxidative phosphorylation toward glycolysis. To verify this, the expression of glycolysis-related genes PDK1, SLC2A1, HK2, PKM, and GAPDH in bovine pulmonary myofibroblasts was detected by RT-qPCR following exposure to 1% O_2 for 72 h (Figure 4G). Compared with the normoxic control group, the expression of PDK1, SLC2A1, GAPDH, HK2, and PKM at the mRNA level was significantly upregulated in the hypoxia group ($P < 0.05$).

In addition, the intracellular lactate levels were detected using an L-lactate assay kit.

The results showed a significant increase in intracellular lactate levels after 72 hours of culture under 1% O_2 conditions (Figure 4H). Overall, this indicates that the 1% O_2 hypoxic condition promotes energy metabolic reprogramming in bovine pulmonary myofibroblasts, with a marked enhancement of glycolysis.

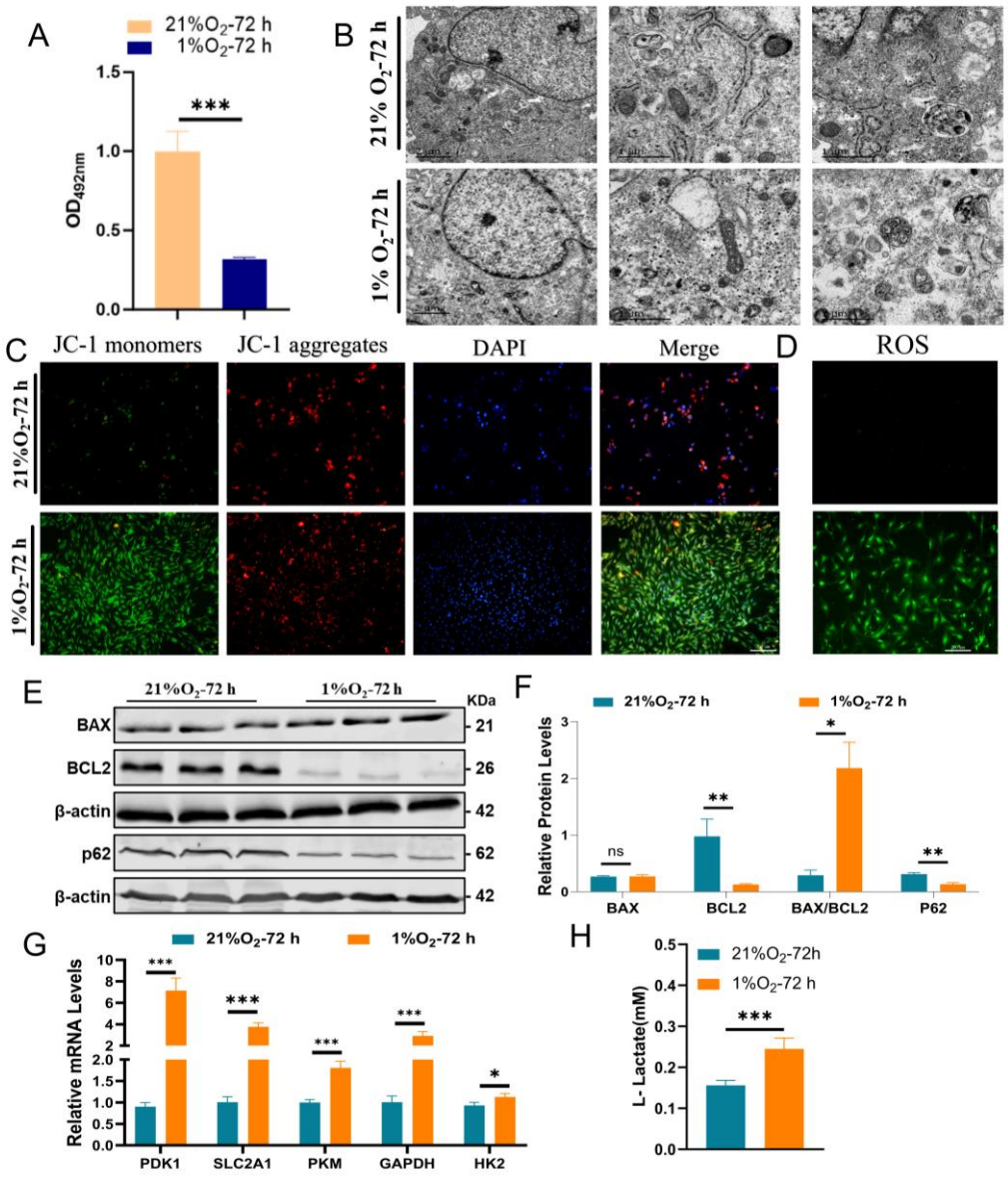


Figure 4. Effects of hypoxia on bovine pulmonary myofibroblasts.

(A) MTT assay showing that cell proliferation was significantly inhibited following treatment with 1% O_2 for 72 h. (B) TEM showing mitochondrial structural and

functional damage, accompanied by a marked increase in the number of autophagosomes, after treatment with 1% O_2 for 72 h. (C) Assessment of mitochondrial membrane potential showing decreased membrane potential, increased green fluorescence, and decreased red fluorescence after 72 h of treatment with 1% O_2. (D) Measurement of intracellular ROS levels showing a significant increase following 72 h of treatment with 1% O_2. (E) Representative western blot images showing relative protein abundances of BAX, BCL2 and p62 in bovine pulmonary myofibroblasts after 72 h exposure to 1% O_2 hypoxic conditions. (F) Quantification of relative protein abundances for BAX, BCL2 and p62 in bovine pulmonary myofibroblasts following 72 h of hypoxic treatment. Data are presented as mean ± SEM. (G) RT-qPCR analysis of the mRNA expression levels of key glycolysis-related genes following72 h of normoxic (21% O_2) or hypoxic (1% O_2) treatment, hypoxia significantly increased the transcriptional levels of PDK1, SLC2A1, PKM, GAPDH, and HK2. (H) Measurement of intracellular lactate levels showing increased lactate accumulation following treatment with 1% O_2 for 72 h (*$P < 0.05$, ***$P < 0.001$).

Result 5: TXNIP Promotes Hypoxia-Induced Apoptosis in Bovine Pulmonary Myofibroblasts

Previous studies have reported that enhanced glycolytic activity and increased lactate production can directly influence chromatin accessibility, thereby modulating gene expression(ref. 42). Based on this, we investigated whether the hypoxia-induced upregulation of TXNIP was associated with enhanced glycolysis and lactate

accumulation. Bovine pulmonary myofibroblasts were treated with the glycolysis inhibitor 2-deoxy-D-glucose (2-DG) under 1% O_2 hypoxic conditions for 72 h the results showed that the expression levels of the glycolysis-related marker genes LDHA and GAPDH were significantly decreased, accompanied by a reduction in intracellular lactate production. Notably, the protein expression levels of E2F1 and TXNIP were also significantly reduced following glycolytic inhibition ($P < 0.05$; Figures. 5A, B). These findings suggest that 2-DG effectively attenuates the hypoxia-induced increase in glycolytic activity and lactate production in bovine pulmonary myofibroblasts and is accompanied by a marked downregulation of E2F1 and TXNIP expression.

To further elucidate the mechanism by which TXNIP regulates apoptosis, the expression of TXNIP-associated downstream proteins in bovine pulmonary myofibroblasts was examined by western blot. Compared with the normoxic control group, exposure to 1% O_2 for 72 h significantly decreased the protein expression of TRX2 ($P < 0.05$), whereas the expression levels of ASK1, p38, and Caspase-3 were significantly increased. In contrast, no significant difference was observed in the expression of phosphorylated ASK1 (p-ASK1) (Figures. 5C, D). These results demonstrate that hypoxic treatment increases TXNIP expression and inhibits TRX2 expression, potentially facilitating the release and activation of ASK1 and subsequent activation of the downstream p38/Caspase-3 signalling axis, thereby promoting apoptosis. To further verify the involvement of TXNIP in this signalling cascade, TXNIP was silenced using siRNA in bovine pulmonary myofibroblasts, followed by

exposure to 1% O_2 for 72 h. and TXNIP and its downstream signalling proteins were detected by western blot. The results showed TXNIP expression was significantly reduced ($P < 0.05$), whereas the expression of TRX2 and p38 were significantly increased ($P < 0.05$). Moreover, the hypoxia-associated increases in Caspase-3, ASK1, and p-ASK1 were no longer statistically significant following TXNIP silencing (Figures. 5E, F). These results indicate that TXNIP depletion alleviates the suppression of TRX2, potentially enhancing TRX2-mediated inhibition of ASK1 and thereby attenuating downstream p38 and Caspase-3 signaling. Collectively, these findings support a pro-apoptotic role for TXNIP in bovine pulmonary myofibroblasts under hypoxic conditions. Consistent with these molecular findings, MTT assays demonstrated that TXNIP silencing significantly increased the proliferative activity of bovine pulmonary myofibroblasts under hypoxic conditions compared with the corresponding control group (Figure. 5G). These results further support the conclusion that TXNIP silencing attenuates hypoxia-associated apoptosis and partially restores cell viability.

To further investigate the effects of TXNIP silencing on cell under hypoxic conditions, transcriptomic sequencing was performed on hypoxia-treated bovine pulmonary myofibroblasts from the TXNIP-silenced group (siTXNIP) and the negative control group (siNC). The quality-control results indicated that the RNA-seq datasets were of sufficient quality for subsequent downstream analyses (Supplementary Table 1). Following siRNA-mediated silencing, TXNIP expression was markedly reduced,

accompanied by a reversal of the hypoxia-associated upregulation of MAP3K5 (ASK1), MAPK14 (p38), and CASP3 (Caspase-3) (Figure. 5H), consistent with the corresponding changes observed at the protein level. Further analysis of the transcriptomic data revealed that the expression levels of several apoptosis-related genes, including CASP8, CASP9, BAD, BCL2, and BAX, were no longer significantly upregulated following TXNIP silencing (Figure. 5I). In addition, the expression of the pro-apoptotic gene BAK1 was significantly decreased ($P < 0.05$). Collectively, these findings indicate that TXNIP silencing attenuates the activation of apoptosis-associated molecular responses under hypoxic conditions, supporting a role for TXNIP in promoting hypoxia-induced apoptosis in bovine pulmonary myofibroblasts.

Using $|\log_2 FC| \geq 1$ and $P < 0.05$ as the screening criteria, cellular transcriptomic data were further analyzed, and 420 significantly differentially expressed genes (DEGs) were identified. GO functional enrichment analysis identified 114 terms, of which 69 were significantly enriched. Among these, 22, 24, and 23 terms were associated with the Molecular Function (MF), Biological Process (BP), and Cellular Component (CC) categories, respectively, following TXNIP silencing under hypoxic conditions (Figure. 5J). Within the BP category, significantly enriched terms included collagen fibril organization, extracellular matrix organization, positive regulation of cell migration, cellular response to oxidative stress, vascular endothelial growth factor receptor signaling pathway, and arachidonate metabolic process, among others. Previous studies have shown that vascular endothelial-specific deletion of TXNIP in mice reduces

intracellular oxidative stress, attenuates endothelial inflammation, preserves vascular smooth muscle function, restores vascular vasodilatory capacity, and promotes post-ischaemic angiogenesis and blood-flow recovery. Consistent with these findings, the enrichment of pathways related to arachidonate metabolism following TXNIP silencing suggests that TXNIP deficiency under hypoxic conditions may alleviate intracellular oxidative stress and contribute to the remodeling of cellular lipid metabolism. In the CC category, significantly enriched terms included extracellular region, axon, extracellular space, and membrane. The enrichment of DEGs in membrane- and extracellular matrix-associated compartments suggests that TXNIP deficiency can block the transmission of oxidative stress and vascular remodeling signals between the intracellular and extracellular environments by repairing membrane structure and inhibiting abnormal synthesis of the extracellular matrix. In the MF category, significantly enriched terms included growth factor activity, calcium channel activity, metal ion binding, kinase binding, and cytokine activity. Previous studies have reported that zinc ion binding can negatively regulate TXNIP expression. The enrichment of the metal ion binding term following TXNIP silencing suggests that TXNIP deficiency may contribute to the restoration of intracellular ion homeostasis, thereby limiting ROS generation and alleviating hypoxia-induced oxidative stress and pulmonary vascular injury. In addition, the significant enrichment of terms related to kinase interactions suggests that TXNIP can inhibit the signaling of multiple kinases, thereby blocking hypoxia-induced endothelial activation and cell apoptosis. KEGG pathway analysis

identified 30 enriched pathways, of which 16 were significantly enriched. Among these, 11 pathways closely associated with TXNIP-mediated regulation under hypoxic conditions are presented in Figure. 5K. TXNIP has been reported to promote pro-apoptotic MAPK signaling by suppressing Akt phosphorylation and enhancing ROS accumulation. Thus, elevated TXNIP expression under hypoxic conditions can attenuate the cytoprotective effects mediated by Akt while amplifying oxidative stress-associated injury through MAPK signaling. In addition, hypoxia-induced TXNIP accumulation can activate Wnt and Rap1 signaling through increased intracellular ROS levels, potentially contributing to abnormal pulmonary vascular proliferation and excessive collagen deposition. In contrast, TXNIP knockdown alleviates hypoxia-associated structural disorder of pulmonary vascular and excessive remodeling of extracellular matrix. TXNIP silencing may attenuate hypoxia-induced oxidative injury and apoptosis in pulmonary cells through multiple regulatory mechanisms involving cell survival, oxidative stress, and vascular remodeling. These transcriptomic findings are consistent with the protein-level results showing attenuation of the pro-apoptotic effects after TXNIP silencing, and further suggest that TXNIP depletion can enhance cellular antioxidant capacity under hypoxic conditions.

Among the 420 DEGs, 116 were upregulated and 304 were downregulated. GO and KEGG enrichment analyses were subsequently performed separately for the upregulated and downregulated genes. The 116 upregulated genes were enriched in 58 GO terms, of which 34 were significantly enriched, including 5 MF, 25 BP, and 4 CC

terms. In addition, four pathways were significantly enriched by KEGG analysis. Among the 304 downregulated genes, 100 GO terms were enriched, of which 64 were significant, including 15 MF, 32 BP, and 17 CC terms, along with 15 significantly enriched KEGG pathways（Figure. 5L）. The upregulated genes were significantly enriched in biological processes related to the innate immune response, calcium-mediated signaling, chemotaxis, and cell differentiation. At the cellular component level, these genes were predominantly associated with the extracellular region and plasma membrane, whereas the enriched molecular functions mainly included calcium ion binding, growth factor activity, and nucleic acid endonuclease activity. These enrichment patterns suggest that TXNIP silencing may alleviate mitochondrial ROS accumulation and relieve the inhibition of calcium channels, innate immunity, and chemotactic signals, reshape the transcription of genes related to cell membrane and extracellular matrix, and thereby regulate the differentiation and hypoxia adaptation process of bovine pulmonary myofibroblasts. In contrast, the downregulated genes were predominantly enriched in biological processes associated with transmembrane transport, adipocyte differentiation, and receptor-mediated endocytosis. The enriched cellular components mainly included membrane structures, extracellular regions, synapse, axon, and dendrite, with a relatively large number of genes involved. The major enriched molecular functions included metal ion binding, calcium channel activity, and collagen binding. Previous studies have shown that sustained hypoxia-induced excessive ROS can trigger cells to upregulate membrane transport, metal ion

antioxidant-related genes to compensate for oxidative damage. Thus, TXNIP silencing can significantly alleviate intracellular oxidative stress levels, leading to the synchronous downregulation of the compensatory processes, neurodevelopment-related programs, and collagen-binding molecules associated with profibrotic effects.

Taken together, the enrichment profiles indicate that TXNIP silencing under hypoxic conditions enhances the adaptive capacity of bovine pulmonary myofibroblasts to extreme hypoxic environments by activating calcium signaling, innate immune responses, and cell differentiation pathways. On the other hand, it alleviates mitochondrial oxidative damage by downregulating membrane transport, metal ion antioxidant, and collagen-binding related pathways.

Further analysis of the significantly enriched KEGG signaling pathways of up- and down-regulated genes revealed that the core pathways enriched by down-regulated DEGs are primarily classical hypoxia response pathways such as the calcium signaling pathway, MAPK, PI3K-Akt, Rap1, and cAMP. In addition, pathways related to neuroactive ligand–receptor interactions, ECM–receptor interactions, Wnt and Ras signalling were also significantly enriched. Previous studies have demonstrated that TXNIP can promote sustained activation of the MAPK and PI3K-Akt signalling cascades through the accumulation of mitochondrial ROS, thereby contributing to hypoxia-induced suppression of pulmonary fibroblast proliferation, excessive collagen deposition and fibrotic remodelling. TXNIP silencing can alleviate intracellular oxidative stress and consequently attenuate the transcriptional activation of these

injury- and fibrosis-associated signalling pathways. Meanwhile, the concomitant downregulation of the calcium signalling pathway may reflect a reduction in the compensatory calcium-dependent response to hypoxic stress. In contrast, the up-regulated genes were significantly enriched in only four TXNIP-associated pathways, namely the NF-κB signalling pathway, calcium signalling pathway, cell adhesion molecule interactions, and transcriptional dysregulation in cancer. Previous studies have shown that TXNIP can suppress NF-κB nuclear translocation and thereby restrain the transcription of downstream genes involved in innate immune and inflammatory chemotactic responses. Thus, TXNIP silencing may relieve this inhibitory effect and enhance NF-κB-mediated adaptive inflammatory responses under hypoxic conditions. Concurrent modulation of calcium signalling and cell adhesion molecule-related pathways may further contribute to the maintenance of cellular homeostasis and adaptation to hypoxic stress. From the above results, it can be inferred that TXNIP, as an upstream core regulatory molecule, participates in the homeostatic remodeling of bovine pulmonary myofibroblasts under hypoxic conditions by bidirectionally regulating the MAPK/PI3K-Akt pro-injury pathway and the NF-κB adaptive protective pathway.

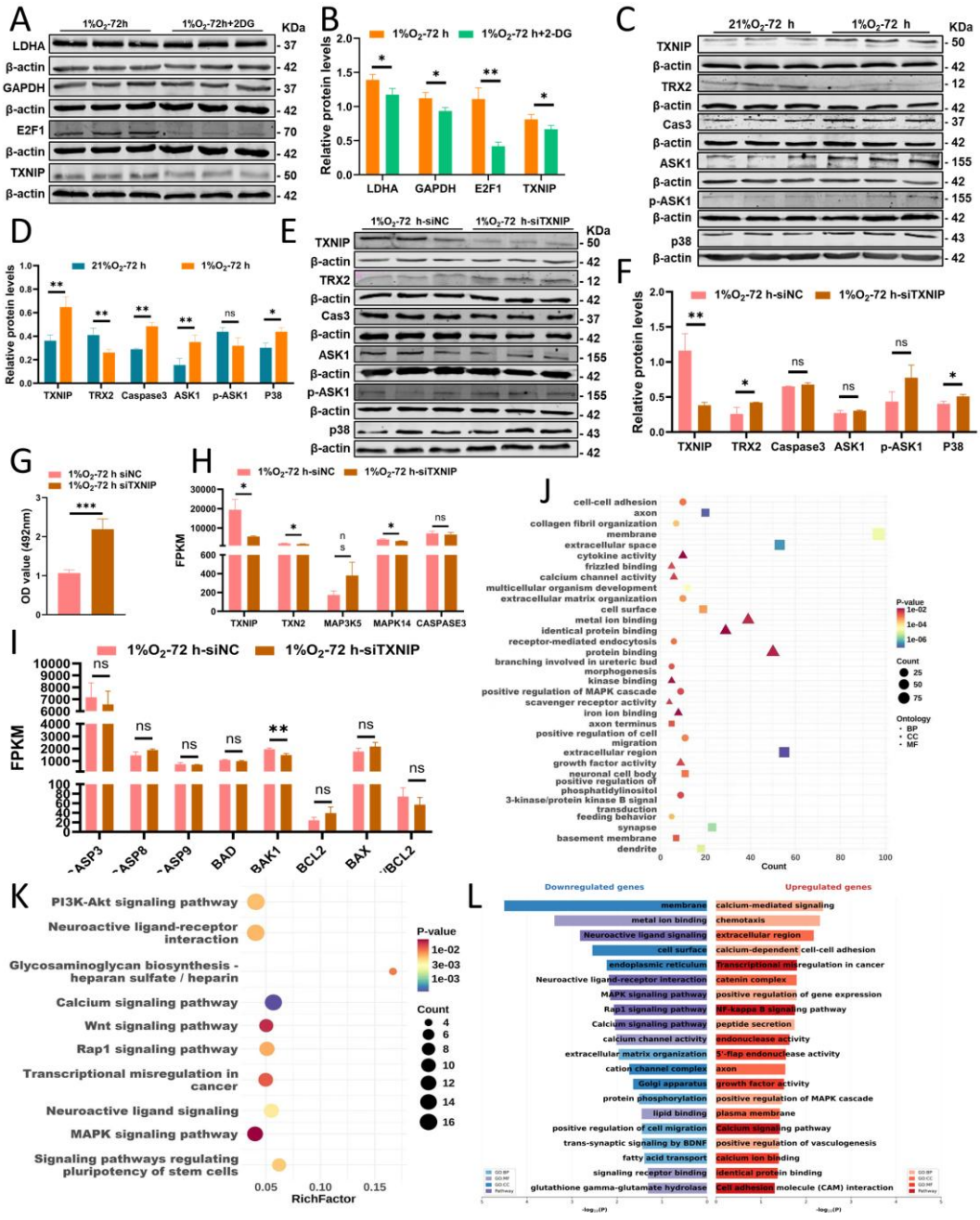


Figure 5. TXNIP promotes apoptosis in bovine pulmonary myofibroblasts under hypoxic conditions.

(A) Representative western blot images showing protein abundances of LDHA, GAPDH, E2F1 and TXNIP in bovine pulmonary myofibroblasts treated with the glycolysis inhibitor 2-DG under 1% O_2 hypoxic conditions. (B) Quantification of

relative protein abundances for LDHA, GAPDH, E2F1 and TXNIP in bovine pulmonary myofibroblasts after 2-DG treatment under 1% O_2 hypoxic conditions. (C) Representative western blot images showing relative protein abundances of TXNIP, TRX2, ASK1, p38 and Caspase-3 in bovine pulmonary myofibroblasts after 72 h exposure to 1% O_2 hypoxic conditions. (D) Quantification of relative protein abundances for TXNIP, TRX2, ASK1, p38 and Caspase-3 in bovine pulmonary myofibroblasts following 72 h of hypoxic treatment. Data are presented as mean ± SEM.

(E) Representative western blot images showing relative protein abundances of TXNIP and its downstream effectors TRX2, ASK1, p38 and Caspase-3 in bovine pulmonary myofibroblasts upon TXNIP knockdown under 1% O_2 hypoxic conditions.

(F) Quantification of relative protein abundances for TXNIP, TRX2, ASK1, p38 and Caspase-3 in bovine pulmonary myofibroblasts following TXNIP knockdown under 1% O_2 hypoxic conditions. Data are presented as mean ± SEM. (G) MTT assay showing that TXNIP knockdown alleviates the hypoxia-induced reduction in cell viability. (H–I) Transcriptomic FPKM analysis showing that TXNIP knockdown attenuates the transcriptional activation of stress- and apoptosis-related genes under hypoxic conditions. (J–K) Significantly enriched GO terms and KEGG pathways identified from the transcriptomic analysis. (L) Significantly enriched GO terms and KEGG pathways among up- and down-regulated genes identified from the transcriptomic analysis. *P < 0.05, **P < 0.01, ***P < 0.001; ns, not statistically significant.

Discussion

This study integrated ATAC-seq and RNA-seq data to systematically analyzed changes， in chromatin accessibility and gene expression associated with hypoxic adaptation in the lung tissues of plateau cattle and plain cattle. Significant differences in chromatin accessibility were identified between the two groups, with 6,508 DARs detected and 560 DAR-associated genes annotated. The functions of these genes were primarily annotated to pathways closely related to hypoxic adaptation, including VEGF, cellular senescence, apoptosis, autophagy, PI3K-Akt, NOD-like receptor and MAPK signalling pathways. Furthermore, 13 key genes related to hypoxic adaptation of bovine lung tissue were screened including TXNIP, NRP1, B2M and NEDD4L，and others. Building on these findings, bovine pulmonary myofibroblasts were subsequently used as an in vitro hypoxia model to investigate the hypoxia effects and to elucidate the role and underlying mechanism of the key gene TXNIP. The results demonstrated that hypoxic exposure significantly inhibited the proliferative activity of bovine pulmonary myofibroblasts, and induced ultrastructural damage to intracellular organelles, including mitochondria and the endoplasmic reticulum, and was also accompanied by a reduction in mitochondrial membrane potential and an increase in intracellular ROS levels. Further investigation revealed that hypoxic exposure increased intracellular lactate levels and enhanced histone lactylation, which in turn promoted chromatin openness and the expression of the transcription factor E2F1. E2F1 subsequently positively regulates the transcriptional activation of TXNIP, resulting in increased TXNIP expression. Elevated TXNIP then interacted with mitochondrial TRX2, thereby

facilitating the release of ASK1 and promoting downstream p38 signalling, followed by activation of caspase-3 and induction of apoptosis in pulmonary cells. Collectively, these findings support a model in which the lactate–histone lactylation–E2F1–TXNIP axis contributes to the cellular response to hypoxic stress and provide evidence that TXNIP plays a critical role in regulating hypoxia-associated apoptosis in bovine pulmonary cells, Figure 6**.**

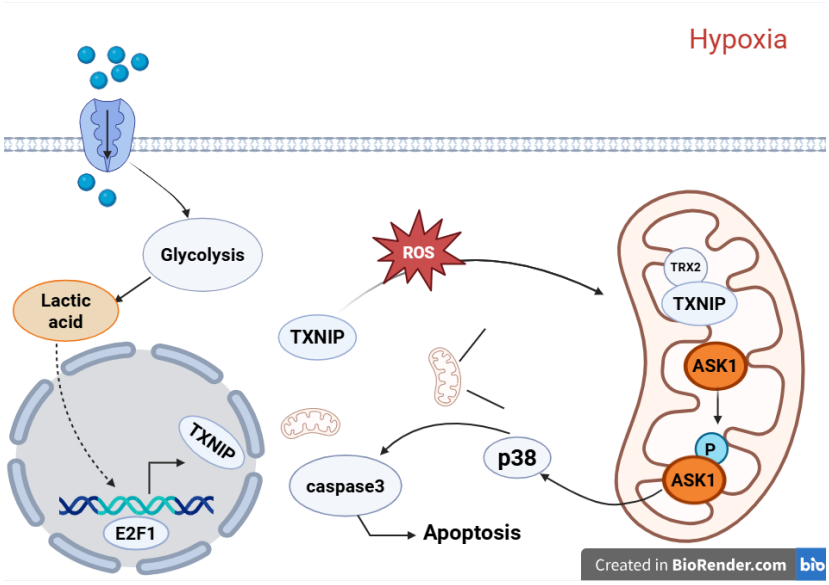


Figure 6. Schematic illustration of the proposed mechanism by which chromatin-accessibility-associated E2F1-TXNIP axis mediates pulmonary hypoxic adaptation in highland cattle.

Chromatin accessibility is a key component of epigenetic regulation; it reflects the binding status of transcription factors to cis-regulatory elements and serves as a powerful tool for elucidating transcriptional reprogramming in response to hypoxia. The insertion fragment distribution, TSS enrichment, and genomic annotation features in the ATAC-seq data of this study are consistent with the published ATAC-seq results

of mammals such as pigs and cattle(ref. 43, 44, 45, 46, 47), confirming the reliability of the sequencing data. Open chromatin regions in bovine lung tissue were primarily enriched in promoters (especially those < 1 kb), intergenic regions, and intron regions, consistent with reports from other mammals, suggesting that hypoxia-mediated chromatin remodeling occurs preferentially in core transcriptional regulatory regions, and that this distribution pattern is relatively conserved across mammals(ref. 43, 44). DARs analysis revealed that hypoxic environment induces large-scale chromatin remodeling in the lungs of high-altitude cattle, characterized by predominantly upregulated and secondarily downregulated changes. This process enhances chromatin accessibility of hypoxia-responsive genes by activating silenced or low-activity regulatory elements, thereby mediating pulmonary hypoxic adaptation. In contrast to the Tibetan population's adaptation pattern, which tends toward chromatin closure and simplification(ref. 48). Domesticated and wild high-altitude mammals largely rely on positive regulatory strategies involving chromatin opening to achieve environmental adaptation(ref. 49, 50, 51). Previous studies on yaks, high-altitude pikas,and hypoxic rat smooth muscle cells under hypoxia have also observed chromatin opening(ref. 2, 52, 53), suggesting that high-altitude adaptation exhibits species-specific epigenetic preferences.

GO and KEGG enrichment analyses indicate that genes associated with DARs are significantly enriched in classic hypoxic response pathways such as PI3K-Akt, AMPK ,MAPK, HIF-1, and apoptosis, consistent with previous findings on hypoxic

stress, vascular remodeling, and cellular homeostasis in mammalian lungs(ref. 54). The VEGF pathway participates in pulmonary vascular remodeling to optimize oxygen delivery; the FOXO pathway synergistically regulates antioxidant capacity and BIM-mediated apoptosis, balancing cell survival and death(ref. 55, 56). The PI3K-Akt and MAPK pathways constitute a core survival regulatory axis that antagonizes the pro-apoptotic effects of FOXO, thereby maintaining cell proliferation and survival under hypoxic conditions(ref. 57).The AMPK–mTOR pathway suggests that hypoxia triggers energy reprogramming, maintaining basal energy supply by inhibiting protein synthesis and promoting glycolysis(ref. 58) . The enrichment of apoptosis-autophagy pathway reflects that autophagy can clear damaged mitochondria and alleviate oxidative damage, and NOD/Toll-like receptor inflammatory pathway exerts bidirectional effects: moderate activation contributes to the body's adaptation, whereas excessive activation exacerbates lung tissue damage(ref. 58, 59). These pathways synergistically construct a multilevel hypoxic adaptation network in the lung: VEGF pathway mediates oxygen supply remodeling, FoxO/PI3K-Akt pathway regulates cell fate, and AMPK–mTOR facilitates metabolic adaptation. At the same time, ROS-induced mitochondrial stress can activate the PI3K-Akt-HIF-1α pathway to initiate a hypoxic response, while HIF-1 and MAPK in turn counteract ROS accumulation, forming a negative feedback regulatory loop Calcium signaling and apoptosis pathways collectively suggest that ion homeostasis and cell fate regulation are also involved in the processes of damage and remodeling in high-altitude lung tissue(ref. 60, 61, 62, 63).

The effects of hypoxia on ROS production remain debated and appear to depend on species, oxygen concentration, and cell type. In this study, the proliferation of bovine pulmonary myofibroblasts was significantly inhibited, mitochondrial membrane potential decreased, and intracellular ROS accumulated extensively under 1% O_2 hypoxic conditions, which is consistent with the results of severe hypoxia models in human smooth muscle cells and pulmonary interstitial cells(ref. 64, 65, 66). However, some studies have shown that the level of ROS in osteosarcoma cells decreases under 0.5% O_2 conditions. It suggests that insufficient oxygen substrate in extremely hypoxic environments limits the production of superoxide anions, indicating that the hypoxia effects on cell are condition-dependent(ref. 66). Mitochondria are the core organelles for energy metabolism and ROS production. Under normoxic conditions, bovine pulmonary myofibroblasts exhibited intact mitochondrial morphology and well-defined cristae. Continuous 1% O_2 hypoxic stress resulted in mitochondrial swelling, disruption and fragmentation of cristae, and a marked reduction in mitochondrial membrane potential. Disruption of mitochondrial structure blocks the electron transport chain, impairs energy metabolism, triggers a burst of ROS. Excessive ROS further damages organelles, amplifies oxidative stress, initiates mitochondrial-dependent intrinsic apoptosis, and ultimately leads to a decrease in cell viability. This cascade of damage is consistent with the conclusions of studies on hypoxic injury in human lung cells(ref. 67, 68, 69, 70).However, mitochondrial responses to hypoxia are determined not only by oxygen availability but also by cell lineage and developmental state. Porcine

embryonic fibroblasts can undergo compensatory mitochondrial remodeling without severe damage under similar hypoxic conditions, suggesting that mitochondria from embryonic cells may have greater stress resistance than those from mature lung stromal cells(ref. 69, 71).

TXNIP is a key molecule that links hypoxic stimulation, oxidative stress, and mitochondrial apoptosis, and has been shown to promote damage in hypoxic models of human and mouse lung cells(ref. 67, 68, 70, 71, 72). This study confirms that hypoxia-induced glycolysis elevation leads to intracellular lactate accumulation, and promotes histone lactylation modification, which contributes to remodeling chromatin accessibility at the TXNIP promoter, facilitates E2F1 binding, thereby promotes TXNIP transcription. Increased TXNIP expression can subsequently promote its mitochondrial interaction with TRX2, leading to the release of ASK1 and activation of the p38/Caspase-3 signaling cascade, ultimately triggering mitochondria-dependent apoptosis. Glycolysis-histone lactylation-target gene activation axis, as a classic metabolic-epigenetic regulatory pattern, has been validated in models of spinal cord injury, retinopathy, and myocardial injury. The glycolysis inhibitor 2-DG can reverse this epigenetic activation effect(ref. 42, 69, 72). In this study, siRNA-mediated interference, inhibitor treatment, and dual-luciferase reporter assays provided evidence that E2F1 directly and positively regulates TXNIP transcription in bovine pulmonary cells, consistent with previous findings in human vascular endothelial progenitor cells(ref. 40). However, the regulatory relationship between E2F1 and TXNIP

dependents on the microenvironment, as E2F1 has also been reported to repress TXNIP expression in the tumor microenvironmen(ref. 38, 39).This study further proved that TXNIP knockdown attenuated hypoxia-induced ROS accumulation, mitochondrial damage, and activation of the ASK1/p38/Caspase-3 pathway in this study. These findings suggest that TXNIP-mediated oxidative stress and mitochondrial apoptosis represent an important molecular mechanism by which mammalian lung cells respond to hypoxia.

This study still has some limitations. For example, ATAC-seq sequencing is based on mixed cell samples of lung tissue, which cannot distinguish the chromatin accessibility features of different cell subpopulations. Additionally, although this study provides evidence that glycolytic activity and E2F1 are involved in the regulation of TXNIP, the precise molecular mechanism by which glycolysis-associated metabolic changes induce chromatin remodeling at the TXNIP promoter remains unclear.

Materials and Methods

3.1. Animals and Ethics

Bovine lung tissue was collected from young humped cattle (16 months old, n = 5) in the Shigatse Prefecture of the Tibet Autonomous Region (altitude 3,500 m) and from young Jinnan cattle (15 months old, n = 5) at the National Genetic Resource Conservation Center for Jinnan Cattle in Yuncheng City, Shanxi Province (altitude 350 m). All animals were clinically healthy males; only male animals were used to eliminate potential confounding effects of sex hormones, consistent with standard practice in this

field. Lung tissue samples for ATAC-seq and RNA-seq were placed in pre-chilled cryovials immediately after collection and rapidly frozen in liquid nitrogen. All experimental procedures were conducted in accordance with the animal ethics guidelines of the People's Republic of China.

3.2. ATAC-seq Library Preparation and Sequencing

Lung tissue was collected from five Jinnan cattle and five humped cattle (10 samples in total) for ATAC-seq library construction. The transposition mixture containing transposase and two equimolar adapters (Adapter 1 and Adapter 2) was added into quality-controlled preprocessed samples, followed by incubation at 37 °C for 30 min to simultaneously perform transposition and ligate the adapters to the ends. After primer amplification and purification, the resulting fragmented products constituted the final sequencing library. Sequencing was subsequently performed by Novogene using the Illumina NovaSeq 6000 platform.

Raw sequencing reads from all samples were first assessed for quality using FastQC, and fastp software was used to remove adapters and low-quality sequences. Prior to alignment, a reference genome index was constructed, and Bowtie2 was used to align reads to the reference genome (Bos taurus ARS-UCD1.2). The resulting SAM files were converted to BAM format using SAMtools. BAM files were filtered through a two-step process using Sambamba and SAMtools; after removing mitochondrial and low-quality reads, PCR duplicates were removed using SAMtools markup. Peak calling was performed with MACS2 to identify open chromatin regions. The distribution of peaks

across different genomic regions was evaluated using ChIPseeker. All BigWig files were visualized using the Integrative Genomics Viewer (IGV). Differential peak analysis between groups was conducted using the DiffBind package in R, with thresholds of $|\log2(\text{fold change})| \geq 1$ and $p < 0.05$. ATAC-seq peaks were annotated using HOMER's annotatePeaks.pl tool. Motif predictions for differentially accessible sequences in the promoter regions of key candidate genes were performed using the JASPAR database.

3.3.RNA-seq

Total RNA was extracted using TRIzol reagent according to the manufacturer's instructions from five lung tissue samples of humped cattle and Jinnan cattle respectively, as well as from three bovine pulmonary myofibroblast samples per group from the TXNIP-interference group and the corresponding control group after 72 h of exposure to 1% O_2. RNA integrity was assessed using an Agilent 2100 Bioanalyzer (Agilent Technologies, CA, USA), and RNA-seq libraries were subsequently constructed. Library quality was evaluated using a high-sensitivity DNA assay kit, and sequencing was performed on the Illumina HiSeq 4000 platform at Meilun Biotechnology. Reads were mapped to the bovine reference genome (Bos taurus ARS-UCD1.2) using HISAT2. Differentially expressed genes (DEGs) were analyzed separately between lung tissues from humped cattle and Jinnan cattle, and between hypoxic cells with and without TXNIP interference using DESeq2.

3.4. Isolation, Characterization, and Hypoxia Induction of Primary Lung Cells

Distal lung tissue was harvested from 15-day-old Holstein calves, rinsed aseptically, stripped of the pleura, and minced into fragments not exceeding 3 mm^3. The minced tissue was transferred to 50-mL centrifuge tubes, each filled to the 5-mL scale line, and washed repeatedly with sterile DPBS (pH 7.4) supplemented with 100 U/mL penicillin and 100 U/mL streptomycin. After removal of the supernatant, a digestion mixture containing of 0.008% elastase, 0.2% collagenase, 0.005% DNase I, and 0.05% trypsin was added, and enzymatic digestion was carried out at 37 °C for 30 min with gentle shaking. The resulting suspension was sequentially passed through sterile cell strainers with pore sizes of 100 μm, 50 μm, and 25 μm. The filtrate was collected in a 50-mL centrifuge tube and centrifuged at 300 × g for 10 min. The cell pellet was resuspended in DMEM/F12 medium supplemented with 10% fetal bovine serum and 1% penicillin-streptomycin, and the resulting cell suspension was seeded into culture vessels to obtain primary cells. Immunophenotypic characterization cell dentification was performed using immunofluorescence with antibodies against α-smooth muscle actin (α-SMA) and vimentin; the positive rates for both markers exceeded 95%, confirming that the isolated cells were primary bovine pulmonary myofibroblasts (Supplementary Figure 1). Cells at passage 4 exhibiting stable morphology were subjected to either hypoxic (1% O_2) or normoxic (21% O_2) conditions for 72 h, after which the cells were harvested for subsequent analyses.

3.5. MTT

Logarithmic-phase bovine pulmonary myofibroblasts were seeded in 96-well plates

under basal culture conditions as described above. At the end of the treatment period, 10 μL of MTT reagent was added to each well, followed by incubation for 4 h under normoxic conditions. The culture medium was then carefully removed, and 150 μL of DMSO was added to each well. The plates were gently shaken at low speed for 10 min to ensure complete dissolution of the formazan crystals. Absorbance was subsequently measured at 490 nm using a microplate reader.

3.6. Transmission Electron Microscopy (TEM)

Bovine pulmonary myofibroblasts in the logarithmic growth phase were seeded into 10-cm culture dishes, with basal culture conditions as described above. At the end of the incubation period, the cells were harvested and immediately fixed in 2% paraformaldehyde and 2.5% glutaraldehyde for 2 h, followed by post-fixation with 1% osmium tetroxide (OsO_4) at 4 °C for 2 h. The specimens were subsequently dehydrated through a graded ethanol series (50%, 70%, 90%, and 100%), embedded in Epon 812 epoxy resin, and polymerized. Ultrathin sections were then prepared and stained with 2% uranyl acetate and 0.2% lead citrate. The ultrastructural features of bovine pulmonary myofibroblasts were examined and photographed using a JEM-1400 transmission electron microscope (JEOL, Japan) operated at an accelerating voltage of 80 kV.

3.7. Mitochondrial Membrane Potential Assay

Logarithmic-phase bovine pulmonary myofibroblasts were seeded into 3.5-cm culture dishes under basal culture conditions as described above. Mitochondrial

membrane potential (ΔΨm) was assessed using a JC-1 Mitochondrial Membrane Potential Assay Kit (Beyotime Biotechnology, China) according to the manufacturer's instructions. Briefly, the JC-1 staining working solution was prepared according to the manufacturer's protocol. Subsequently, 1 mL of JC-1 staining working solution was added to each dish, and the cells were gently mixed and incubated at 37 °C for 20 min. The staining solution was then aspirated, and the cells were washed twice with JC-1 staining buffer. The fluorescence signals were subsequently examined using a fluorescence microscope.

3.8. Reactive Oxygen Species （ROS） Assessment

Logarithmic-phase bovine pulmonary myofibroblasts were seeded into 3.5-cm culture dishes under basal culture conditions as described above. Prior to probe loading, DCFH-DA was diluted 1:1000 in serum-free culture medium to a final concentration of 10 μM. The culture medium was then aspirated, and 1 mL of the DCFH-DA working solution was added to each dish. The cells were incubated at 37 °C for 30 min in the dark. Subsequently, the cells were washed twice with serum-free culture medium to remove excess DCFH-DA that had not entered the cells. Intracellular fluorescence was subsequently examined using a fluorescence microscope.

3.9. RT-qPCR

Logarithmic-phase bovine pulmonary myofibroblasts were seeded into 6-well plates under basal culture conditions as described above. Total RNA was extracted using TRIzol reagent. RNA was subsequently reverse-transcribed into complementary DNA

(cDNA) using the FastKing cDNA First-Strand Synthesis Kit (Tiangen Biotech, China) according to the manufacturer's instructions. RT-qPCR was performed using the FastFire Rapid Fluorescent Quantitative PCR Premix Kit (SYBR Green; FP207) according to the manufacturer's instructions. The primers were synthesized by GenScript Biotech (Shanghai) Co, Ltd, China.

3.10. Lactate Level Assay

Logarithmic-phase bovine pulmonary myofibroblasts were seeded into 3.5-cm culture dishes under basal culture conditions as described above. Following the incubation period, lactate levels in each dish were determined using an L-lactate Assay Kit based on the WST-8 method, according to the manufacturer's instructions. Three independent replicates were included for each experimental group to ensure the reliability and reproducibility of the results.

3.11. Treatment with Cell Inhibitors

For E2F1 inhibition experiment, the E2F1 inhibitor HLM006474 was added directly to the complete culture medium to achieve a final concentration of 60 μM. The corresponding control group received an equivalent volume of DMSO. The cells were subsequently maintained under normoxic conditions (21% O_2) for 72 h, after which the cells were harvested for subsequent analyses.

For glycolysis inhibition experiment, 2-deoxy-D-glucose (2-DG) was dissolved in sterile PBS and subsequently diluted in complete culture medium to a final concentration of 1 mM. An equivalent volume of DMSO was added to the

corresponding control group. The cells were then maintained under normoxic conditions (21% O_2) for 72 h, followed by cell harvesting for subsequent analyses.

3.12. Western Blot Analysis of Protein Expression

Total proteins were extracted from bovine pulmonary myofibroblasts using RIPA lysis buffer and centrifuged at 12,000 × g for 10 min at 4 °C. The supernatants were collected, and total protein concentrations were determined using a BCA Protein Assay Kit (Beyotime Biotechnology, China) according to the manufacturer's instructions. Equal amounts of protein samples were mixed with 5× loading buffer and denatured at 99 °C for 10 min in a metal heating block. The denatured proteins were separated by SDS-PAGE at 65 V for 45 min, followed by electrophoresis at 120 V for 80 min, and subsequently transferred onto PVDF membranes at 0.22 A for 1 h. The membranes were blocked with 5% skimmed milk in TBST for 1 h at room temperature and then incubated overnight at 4 °C with the following primary antibodies: Bax (21 kDa, 1:1000), BCL2 (26 kDa, 1:1000), p62 (62 kDa, 1:1000), LC3B (14 and 16 kDa, 1:2000), TXNIP (50 kDa, 1:1000), TRX2 (14 kDa, 1:800), ASK1 (155 kDa, 1:500), p38 (43 kDa, 1:500), phosphorylated ASK1 (p-ASK1; 155 kDa, 1:500), caspase-3 (37 kDa, 1:500), E2F1 (70 kDa, 1:750), LDHA (37 kDa, 1:3000), GAPDH (37 kDa, 1:2000), and β-actin (42 kDa, 1:2000). Following primary antibody incubation, the membranes were washed three times with 1× TBST for 5 min each on a shaker and then incubated with the appropriate secondary antibody (1:10,000) for 1 h at room temperature with gentle agitation. The membranes were subsequently washed three times with 1× TBST for 10 min each.

Protein bands were visualized using an appropriate chemiluminescence detection system, and band intensities were quantified using ImageJ software. The relative expression level of each target protein was calculated by normalizing the densitometric value of the target protein band to that of the corresponding β-actin band.

3.13. Cell Transfection

Small interfering RNAs (siRNAs) targeting TXNIP and E2F1, together with a negative control siRNA (siNC), were synthesized by Shengong Bioengineering (Shanghai), China. When bovine pulmonary myofibroblasts reached approximately 70–80% confluence, the culture medium was replaced with Opti-MEM and the cells were preincubated for 4 h. siRNA transfection was subsequently performed in 24-well and 6-well plates using Lipofectamine 3000 according to the manufacturer's instructions. Six hours after transfection, the transfection medium was replaced with complete culture medium. The cells were then maintained under normoxic (21% O_2) or hypoxic (1% O_2) conditions for 72 h. At the end of the incubation period, the cells were harvested for subsequent RNA and protein extraction.

3.14. Dual-Luciferase Reporter Assay

A dual-luciferase reporter assay was performed to investigate the regulatory relationship between E2F1 and the TXNIP promoter. The wild-type (WT) TXNIP promoter containing the putative E2F1-binding site and the corresponding mutant (MT) promoter were generated and cloned into the pGL3-Basic luciferase reporter vector following digestion with MluI and XhoI. Bovine pulmonary myofibroblasts were co-

transfected with the WT or MT TXNIP promoter reporter plasmid together with the appropriate Renilla luciferase internal control plasmid. At 24 h after transfection, luciferase activities were measured using a dual-luciferase reporter assay system according to the manufacturer's instructions. The firefly luciferase activity was normalized to Renilla luciferase activity, and the relative luciferase activity was calculated accordingly.

3.15. Statistical Analysis

All experiments were independently repeated at least three times. Statistical analyses were performed using GraphPad Prism 8.0 (GraphPad Software, USA). Data are presented as the mean ± standard error of the mean (SEM). Comparisons between two groups were performed using an unpaired two-tailed Student's t-test, whereas comparisons among multiple groups were performed using one-way analysis of variance (ANOVA). A P value < 0.05 was considered statistically significant, and a P value < 0.01 was considered highly statistically significant.

Declarations

Ethics approval and consent to participate

Ethics approval was not required for this study. All lung tissue samples were obtained from healthy commercially slaughtered cattle under standard local agricultural practice. All sampling procedures complied with the animal welfare guidelines of the People’s Republic of China.

Consent for publication

Not applicable.

Availability of data and material

Please contact the corresponding author upon reasonable request.

Funding

This study was funded by National Agriculture Key Science & Technology Project (Grant No. NK20221201-6) and the Key Research and Development Program of Xizang Autonomous Region (Grant No. XZ202301ZY0003N)

Authors' contributions

QX and LH conceived and designed the study, supervised the project and obtained funding. MZ performed the ATAC-seq and RNA-seq analyses, the cell experiments and the dual-luciferase assays, and drafted the manuscript. AC and GQMG participated in sample collection and cell isolation. RM and GC performed the RTqPCR and Western blot experiments. YY and JL participated in data analysis and figure preparation. BL and YW provided the animal resources and coordinated tissue sampling. All authors read and approved the final manuscript.

Declaration of competing interest

The authors declare that they have no known competing financial interests or personal relationships that could have appeared to influence the work reported in this paper.

Data availability

Data will be made available on request.

References：

1. Ai H, Yang B, Li J, Xie X, Chen H, Ren J. Population history and genomic signatures for high-altitude adaptation in Tibetan pigs. BMC Genomics. 2014;15(1):834.
2. Gao X, Wang S, Wang YF, Li S, Wu SX, Yan RG, et al. Long read genome assemblies complemented by single cell RNA-sequencing reveal genetic and cellular mechanisms underlying the adaptive evolution of yak. Nat Commun. 2022;13(1):4887.
3. Cui C, Chen S, Mi B, Qi Y, Jiao C, Zhang M, et al. Transcriptomic and Metabolomic Insights into Age-Related Changes in Lung Tissue of Yaks Under Highland Stress. Int J Mol Sci. 2024;25(22).
4. Siques P, Pena E, Brito J, El Alam S. Oxidative Stress, Kinase Activation, and Inflammatory Pathways Involved in Effects on Smooth Muscle Cells During Pulmonary Artery Hypertension Under Hypobaric Hypoxia Exposure. Front Physiol. 2021;12:690341.
5. CHEN Q S， FENG X， JIANG S C. Structural study on plateau adaptability of yak lung. Scientia Agricultura Sinica，2006，10：2107-2113.
6. WEI Q， YU H X， ZHANG Q W， et al. Observation and comparison of alveolar tissue structure in high altitude yaks. Heilongjiang Animal Science and Veterinary Medicine，2011，9：47-49.（in Chinese）
7. ZHANG Y Y， CHEN S W， LI S J， et al. Differential expression of PDK1，HIF-1α and VEGF in the lung of yak （Bos grunniens） at different age. Journal of Agricultural Biotechnology，2023，31（8）： 1623-1631.（in Chinese）
8. Qiu Q, Zhang G, Ma T, Qian W, Wang J, Ye Z, et al. The yak genome and adaptation to life at high altitude. Nat Genet. 2012;44(8):946-9.
9. Wang N, Hua J, Fu Y, An J, Chen X, Wang C, et al. Updated perspective of EPAS1 and the role in pulmonary hypertension. Front Cell Dev Biol. 2023;11:1125723.
10. Wang H, Huang N, Tan M, Zhang X, Chen J, Wei Q. Characteristics of cell adhesion molecules expression and environmental adaptation in yak lung tissue. Sci Rep. 2025;15(1):10914.
11. Li J, Huang N, Zhang X, Sun C, Chen J, Wei Q. Changes of collagen content in lung tissues of plateau yak and its mechanism of adaptation to hypoxia. PeerJ. 2024;12:e18250.
12. NIU Y Y， CUI Y， YU S J， et al. Analysis of JAK2， STAT3， P-JAK2/STAT3 and PCNA proteins expression in the lungs of yaks of different ages. Acta Veterinaria et Zootechnica Sinica，2025，56（6）： 2957-2967.（in Chinese）
13. GE Q Y. Identification of molecular mechanisms associated with high-altitude adaptation in yak lung based on multi-omics analysis. Lanzhou： Gansu Agricultural University，2023.（in Chinese）
14. Yan Z, Yang J, Wei WT, Zhou ML, Mo DX, Wan X, et al. A time-resolved multi-omics atlas of transcriptional regulation in response to high-altitude hypoxia across whole-body tissues. Nat Commun. 2024;15(1):3970.
15. Wang J, Li B, Yang X, Liang C, Raza SHA, Pan Y, et al. Integration of RNA-seq and ATAC-seq identifies muscle-regulated hub genes in cattle. Frontiers in Veterinary Science. 2022;Volume 9 - 2022.
16. Su Y, He S, Chen Q, Zhang H, Huang C, Zhao Q, et al. Integrative ATAC-seq and RNA-seq analysis of myogenic differentiation of ovine skeletal muscle satellite cell. Genomics. 2024;116(3):110851.
17. Xu Z, Wu J, Zhou J, Zhang Y, Qiao M, Sun H, et al. Integration of ATAC-seq and RNA-seq analysis identifies key genes affecting intramuscular fat content in pigs. Front Nutr. 2022;9:1016956.
18. Zhang H, Liu Z, Wang J, Zeng T, Ai X, Wu K. An Integrative ATAC-Seq and RNA-Seq Analysis of the Endometrial Tissues of Meishan and Duroc Pigs. International Journal of Molecular Sciences [Internet]. 2023; 24(19):[14812 p.].
19. Lyu Y, Wang F, Cheng H, Han J, Dang R, Xia X, et al. Recent selection and introgression facilitated high-altitude adaptation in cattle. Science Bulletin.

2024;69(21):3415-3424.
20. Del Console P, Gelsomino L, Giordano C, Pietramala E, Bonofiglio D, Andò S, et al. TXNIP in cancer: Unlocking biological insights and tackling clinical challenges. Biochimica et Biophysica Acta (BBA) - Reviews on Cancer. 2025;1880(5):189394.
21. Kang CW, Nam JH, Oh JH, Wang EK, Lee SH, Shin HJ, et al. Novel mechanism whereby metformin improves glucose homeostasis: TXNIP–GLUT1 axis modulation enhances intestinal glucotonic effects. Experimental & Molecular Medicine. 2025;57(8):1775-1788.
22. Nagakannan P, Islam MI, Sultana S, Karimi-Abdolrezaee S, Eftekharpour E. TXNIP promotes ferroptosis through NCOA4 mediated ferritinophagy. Biochimica et Biophysica Acta (BBA) - Molecular Cell Research. 2025;1872(8):120054.
23. Zhang Y, Li B, Fu Y, Cai H, Zheng Y. Txnip promotes autophagic apoptosis in diabetic cardiomyopathy by upregulating FoxO1 and its acetylation. Cellular Signalling. 2024;124:111469.
24. Lu Y, Li Y, Liu Q, Tian N, Du P, Zhu F, et al. MondoA–Thioredoxin-Interacting Protein Axis Maintains Regulatory T-Cell Identity and Function in Colorectal Cancer Microenvironment. Gastroenterology. 2021;161(2):575-91.e16.
25. Dai X, Liao R, Liu C, Liu S, Huang H, Liu J, et al. Epigenetic regulation of TXNIP-mediated oxidative stress and NLRP3 inflammasome activation contributes to SAHH inhibition-aggravated diabetic nephropathy. Redox Biol. 2021;45:102033.
26. Lv H, Zhu C, Wei W, Lv X, Yu Q, Deng X, et al. Enhanced Keap1-Nrf2/Trx-1 axis by daphnetin protects against oxidative stress-driven hepatotoxicity via inhibiting ASK1/JNK and Txnip/NLRP3 inflammasome activation. Phytomedicine. 2020;71:153241.
27. Wang K, Hu H, Xu Z, Chen Y, Qiu Y, Hu Y, et al. 7-Methoxyflavanone Alleviates LPS-Induced Acute Lung Injury by Suppressing TLR4/NF-κB p65 and ROS/Txnip/NLRP3 Signaling. Biology (Basel). 2025;14(9).
28. Zhang R, Lu M, Ran C, Niu L, Qi Q, Wang H. Ginsenoside Rg1 improves hypoxia-induced pulmonary vascular endothelial dysfunction through TXNIP/NLRP3 pathway-modulated mitophagy. J Ginseng Res. 2025;49(1):80-91.
29. Zhao Y, Chen Y, Liu Z, Zhou L, Huang J, Luo X, et al. TXNIP knockdown protects rats against bupivacaine-induced spinal neurotoxicity via the inhibition of oxidative stress and apoptosis. Free Radical Biology and Medicine. 2024;219:1-16.
30. Wang S-w, Lan T, Zheng F, Huang H, Chen H-f, Wu Q, et al. Celastrol inhibits TXNIP expression to protect pancreatic β cells in diabetic mice. Phytomedicine. 2022;104:154316.
31. Jo SH, Kim MY, Park JM, Kim TH, Ahn YH. Txnip contributes to impaired glucose tolerance by upregulating the expression of genes involved in hepatic gluconeogenesis in mice. Diabetologia. 2013;56(12):2723-2732.
32. Yang S, Guan Y, Zheng C, Xia X, Ma X, Jiang J. FOXO3-induced microRNA-128-3p promotes the progression of spinal cord injury in mice via regulating NLRP3 inflammasome-mediated pyroptosis. Front Immunol. 2025;16:1526721.
33. Wilde BR, Ayer DE. Interactions between Myc and MondoA transcription factors in metabolism and tumourigenesis. Br J Cancer. 2015;113(11):1529-1533.
34. Maimaiti Y, Abulitifu M, Ajimu Z, Su T, Zhang Z, Yu Z, et al. FOXO regulation of TXNIP induces ferroptosis in satellite cells by inhibiting glutathione metabolism, promoting Sarcopenia. Cell Mol Life Sci. 2025;82(1):81.
35. Wang Y, Liu J, Jiang Y, Liu Y, Kuang H, Feng X. KLF5 drives granulosa cell apoptosis and inflammatory injury in polycystic ovary syndrome via transcriptional activation of TXNIP. In Vitro Cell Dev Biol Anim. 2025;61(10):1300-1310.
36. Yan W, Liu M, Qiu M. UPF1 alleviates myocardial ischemia/reperfusion injury via suppressing NLRP3-mediated cardiomyocyte pyroptosis by inhibiting KLF6/TXNIP axis. Int Immunopharmacol. 2026;168(Pt 1):115789.
37. Satsu H, Gondo Y, Shimanaka H, Imae M, Murakami S, Watari K, et al. Signaling Pathway of Taurine-Induced Upregulation of TXNIP. Metabolites. 2022;12(7).
38. Gao S, Bu X, Gao Y, Bao Z, Shi W, Luan L, et al. The miR-532-E2F1 feedback loop contributes to gastric cancer progression. Cell Death Dis. 2022;13(4):376.
39. Knoll S, Fürst K, Kowtharapu B, Schmitz U, Marquardt S, Wolkenhauer O, et al.

E2F1 induces miR-224/452 expression to drive EMT through TXNIP downregulation. EMBO Rep. 2014;15(12):1315-1329.
40. Li J, Ge Z, Li C, Ran H, Zhang Y, Xiang Y. METRNL exerts cytoprotective effects on EPCs via regulation of the E2F1-TXNIP axis in obese limb ischemia. Cellular Signalling. 2025;126:111528.
41. Schieber M, Chandel Navdeep S. ROS Function in Redox Signaling and Oxidative Stress. Current Biology. 2014;24(10):R453-R62.
42. Xi X, Chen Q, Ma J, Wang X, Zhang Y, Xiong Q, et al. Glycolysis-Histone Lactylation Crosstalk Drives TXNIP-NLRP3-Mediated PANoptosome Assembly and PANoptosis Activation Underlying Diabetic Retinopathy Pathogenesis. MedComm (2020). 2025;6(9):e70351.
43. Feng L, Si J, Yue J, Zhao M, Qi W, Zhu S, et al. The Landscape of Accessible Chromatin and Developmental Transcriptome Maps Reveal a Genetic Mechanism of Skeletal Muscle Development in Pigs. International Journal of Molecular Sciences. 2023;24(7):6413.
44. Bai Y, Deng X, Chen D, Han S, Lin Z, Li Z, et al. Integrative analysis based on ATAC-seq and RNA-seq reveals a novel oncogene PRPF3 in hepatocellular carcinoma. Clinical Epigenetics. 2024;16(1):154.
45. Cao X, Cheng J, Huang Y, Lan X, Lei C, Chen H. Comparative Enhancer Map of Cattle Muscle Genome Annotated by ATAC-Seq. Frontiers in Veterinary Science. 2021;Volume 8 - 2021.
46. Tan W, Liu C, Liu J, Wen S, Chen Y, Ren R, et al. Integrative Analysis of ATAC-Seq and RNA-Seq Identifies Key Genes Affecting Muscle Development in Ningxiang Pigs. International Journal of Molecular Sciences. 2025;26(6):2634.
47. Li J, Chen Z, Bai Y, Wei Y, Guo D, Liu Z, et al. Integration of ATAC-Seq and RNA-Seq Analysis to Identify Key Genes in the Longissimus Dorsi Muscle Development of the Tianzhu White Yak. International Journal of Molecular Sciences. 2024;25(1):158.
48. Xin J, Zhang H, He Y, Duren Z, Bai C, Chen L, et al. Chromatin accessibility landscape and regulatory network of high-altitude hypoxia adaptation. Nature Communications. 2020;11(1):4928.
49. Lai D, Qu X, Wang Z, He S, Li X, Bao Q, et al. Integrative Genomic, Transcriptomic and Epigenomic Analysis Reveals cis-regulatory Contributions to High-altitude Adaptation in Tibetan Pigs. Mol Biol Evol. 2025;42(7).
50. Tian X, Ma J, Wu Y, Zhang P, Li Q, Zhang H, et al. Functional analysis of the brain natriuretic peptide gene for high-altitude adaptation in Tibetan pigs. Gene. 2021;768:145305.
51. DOU J J. Identification of conserved non-codingelements in yak genome using ATAC-seq ; Lanzhou University, 2020.（In Chinese）
52. Yu D, Zhang T, Zhou G, Wu Z, Xiao R, Zhang H, et al. Co-profiling reveals distinct patterns of genomic chromatin accessibility and gene expression in pulmonary hypertension caused by chronic hypoxia. Respiratory Research. 2023;24(1):104.
53. An Z, Wei L, Xu B, Wang Z, Gao C, Li J, et al. A homotetrameric hemoglobin expressed in alveolar epithelial cells increases blood oxygenation in high-altitude plateau pika (Ochotona curzoniae). Cell Rep. 2022;41(1):111446.
54. Hu Z, Lu Y, Cai J, Liu J, Wang D. Cross-Oxygen Gradients Transcriptomic Comparison Revealed the Central Role of MAPK and Hippo in Hypoxia-Mediated Mammary Proliferation Inhibition. Antioxidants (Basel). 2024;13(3).
55. Kudryashova TV, Dabral S, Nayakanti S, Ray A, Goncharov DA, Avolio T, et al. Noncanonical HIPPO/MST Signaling via BUB3 and FOXO Drives Pulmonary Vascular Cell Growth and Survival. Circ Res. 2022;130(5):760-778.
56. Chhaing R, Ma Q, Schuh M, Erkan E. Downregulation of Akt induces proximal tubule epithelial cell apoptosis via Foxo-1-BIM pathway in proteinuric states. Res Sq. 2025.
57. Wang H, Wang G, Meng Y, Liu Y, Yao X, Feng C. Modified Guo-Min decoction ameliorates PM2.5-induced lung injury by inhibition of PI3K-AKT and MAPK signaling pathways. Phytomedicine. 2024;123:155211.
58. Li Y, Sun Y, Wang J, Wang X, Yang W. Voacangine protects hippocampal neuronal

cells against oxygen-glucose deprivation/reoxygenation-caused oxidative stress and ferroptosis by activating the PI3K-Akt-FoxO signaling. J Appl Toxicol. 2024;44(8):1246-1256.
59. Zhou S, Sun J, Zhu W, Yang Z, Wang P, Zeng Y. Hypoxia studies in non-small cell lung cancer: Pathogenesis and clinical implications (Review). Oncol Rep. 2025;53(2):29.
60. Al-Faze R, Ahmed HA, El-Atawy MA, Zagloul H, Alshammari EM, Jaremko M, et al. Mitochondrial dysfunction route as a possible biomarker and therapy target for human cancer. Biomed J. 2025;48(1):100714.
61. Li X, Tian X, Liu T, Li M, Wang W, Wang P, et al. Hydroxytyrosol Alleviated Hypoxia-Mediated PC12 Cell Damage through Activating PI3K/AKT/mTOR-HIF-1α Signaling. Oxid Med Cell Longev. 2022;2022:8673728.
62. Chun Y, Kim J. AMPK–mTOR Signaling and Cellular Adaptations in Hypoxia. International Journal of Molecular Sciences. 2021;22(18):9765.
63. Corrado C, Fontana S. Hypoxia and HIF Signaling: One Axis with Divergent Effects. International Journal of Molecular Sciences. 2020;21(16):5611.
64. Bhansali S, Sohi K, Dhawan V. Hypoxia-induced mitochondrial reactive oxygen species (mtROS) differentially regulates smooth muscle cell (SMC) proliferation of pulmonary and systemic vasculature. Mitochondrion. 2021;57:97-107.
65. Holzwarth C, Vaegler M, Gieseke F, Pfister SM, Handgretinger R, Kerst G, et al. Low physiologic oxygen tensions reduce proliferation and differentiation of human multipotent mesenchymal stromal cells. BMC Cell Biology. 2010;11(1):11.
66. Luo T, Zhu X, Li Y, Cao X, Bai Z, Ma L, et al. Integrated Transcriptomic and Metabolomic Analysis Reveals Myocardial Adaptation Mechanisms in Plateau Pikas (Ochotona curzoniae) at High Altitude. Animals (Basel). 2026;16(15).
67. Zou D, Li J, Fan Q, Zheng X, Deng J, Wang S. Reactive oxygen and nitrogen species induce cell apoptosis via a mitochondria-dependent pathway in hyperoxia lung injury. J Cell Biochem. 2019;120(4):4837-4850.
68. Chuang CY, Chen TL, Cherng YG, Tai YT, Chen TG, Chen RM. Lipopolysaccharide induces apoptotic insults to human alveolar epithelial A549 cells through reactive oxygen species-mediated activation of an intrinsic mitochondrion-dependent pathway. Arch Toxicol. 2011;85(3):209-218.
69. Liu X, Zhao X, Li X, Lv S, Ma R, Qi Y, et al. PM(2.5) triggered apoptosis in lung epithelial cells through the mitochondrial apoptotic way mediated by a ROS-DRP1-mitochondrial fission axis. J Hazard Mater. 2020;397:122608.
70. Sgarbi G, Gorini G, Liuzzi F, Solaini G, Baracca A. Hypoxia and IF1 Expression Promote ROS Decrease in Cancer Cells. Cells. 2018;7(7):64.
71. Mordhorst. -BR, Murphy. -SL, Schauflinger. -M, Salazar. -SR, Ji. -T, Behura. -SK, et al. Porcine Fetal-Derived Fibroblasts Alter Gene Expression and Mitochondria to Compensate for Hypoxic Stress During Culture. Cellular Reprogramming. 2018;20(2018)(4):225-235.
72. Mizuno S, Bogaard HJ, Voelkel NF, Umeda Y, Kadowaki M, Ameshima S, et al. Hypoxia regulates human lung fibroblast proliferation via p53-dependent and -independent pathways. Respiratory Research. 2009;10(1):17.

Supplementary Files

This is a list of supplementary files associated with this preprint. Click to download.

- SupplementaryFigure.docx
- SupplementaryTable.docx
- explanation.pdf
- file.ppt